

1 **Principal component analysis of summertime ground site measurements in the Athabasca oil sands:**

2 **Sources of IVOCs**

3
4 Travis W. Tokarek¹, Charles A. Odame-Ankrah¹, Jennifer A. Huo¹, Robert McLaren², Alex K. Y. Lee^{3, 4},
5 Max G. Adam⁴, Megan D. Willis⁵, Jonathan P. D. Abbatt⁵, Cristian Mihele⁶, Andrea Darlington⁶,
6 Richard L. Mittermeier⁶, Kevin Strawbridge⁶, Katherine L. Hayden⁶, Jason S. Olfert⁷, Elijah G. Schnitzler⁸,
7 Duncan K. Brownsey¹, Faisal V. Assad¹, Gregory R. Wentworth^{5, a}, Alex G. Tevlin⁵, Douglas E. J. Worthy⁶,
8 Shao-Meng Li⁶, John Liggi⁶, Jeffrey R. Brook⁶, and Hans D. Osthoff^{1*}

9
10 [1] Department of Chemistry, University of Calgary, Calgary, Alberta, T2N 1N4, Canada

11 [2] Centre for Atmospheric Chemistry, York University, Toronto, Ontario, M3J 1P3, Canada

12 [3] Department of Civil and Environmental Engineering, National University of Singapore, Singapore
13 117576, Singapore

14 [4] NUS Environmental Research Institute, National University of Singapore, Singapore

15 [5] Department of Chemistry, University of Toronto, Toronto, Ontario, M5S 3H6, Canada

16 [6] Air Quality Research Division, Environment and Climate Change Canada, Toronto, Ontario, M3H 5T4,
17 Canada

18 [7] Department of Mechanical Engineering, University of Alberta, Edmonton, Alberta, T6G 1H9, Canada

19 [8] Department of Chemistry, University of Alberta, Edmonton, Alberta, T6G 2G2, Canada

20 [a] Now at: Environmental Monitoring and Science Division, Alberta Environment and Parks, Edmonton,
21 Alberta, T5J 5C6, Canada

22 * Corresponding author

23

24 *for Atmos. Chem. Phys.*

25 **Abstract**

26 In this paper, measurements of air pollutants made at a ground site near Fort McKay in the Athabasca
27 oil sands region as part of a multi-platform campaign in the summer of 2013 are presented. The
28 observations included measurements of selected volatile organic compounds (VOCs) by a gas
29 chromatograph – ion trap mass spectrometer (GC-ITMS). This instrument observed a large, analytically
30 unresolved hydrocarbon peak (with retention index between 1100 and 1700) associated with
31 intermediate volatility organic compounds (IVOCs). However, the activities or processes that contribute
32 to the release of these IVOCs in the oil sands region remain unclear.

33 Principal component analysis (PCA) with Varimax rotation was applied to elucidate major source types
34 impacting the sampling site in the summer of 2013. The analysis included 28 variables, including
35 concentrations of total odd nitrogen (NO_y), carbon dioxide (CO_2), methane (CH_4), ammonia (NH_3), carbon
36 monoxide (CO), sulfur dioxide (SO_2), total reduced sulfur compounds (TRS), speciated monoterpenes
37 (including α - and β -pinene and limonene), particle volume calculated from measured size distributions
38 of particles less than $10\ \mu\text{m}$ and $1\ \mu\text{m}$ in diameter (PM_{10-1} and PM_1), particle-surface bound polycyclic
39 aromatic hydrocarbons (pPAH), and aerosol mass spectrometer composition measurements, including
40 refractory black carbon (rBC) and organic aerosol components. The PCA was complemented by bivariate
41 polar plots showing the joint wind speed and direction dependence of air pollutant concentrations to
42 illustrate the spatial distribution of sources in the area. Using the 95% cumulative percentage of
43 variance criterion, ten components were identified and categorized by source type. These included
44 emissions by wet tailings ponds, vegetation, open pit mining operations, upgrader facilities, and surface
45 dust. Three components correlated with IVOCs, with the largest associated with surface mining and is
46 likely caused by the unearthing and processing of raw bitumen.

47 **1. Introduction**

48 The Athabasca oil sands region of Northern Alberta, Canada, has seen extraordinary expansion of its oil
49 sands production and processing facilities (CAPP, 2016) and associated emissions of air pollutants over
50 the last several decades (Englander et al., 2013; Bari and Kindzierski, 2015). Air emissions from these
51 facilities have been impacting surrounding communities, including the city of Ft. McMurray and the
52 community of Ft. McKay (WBEA, 2013). To assess the impact of these emissions on human health,
53 visibility, climate, and the ecosystems downwind, it is critical to obtain an understanding of the source
54 types from all activities associated with oil sands operations (ECCC, 2016).

55 Prior to 2013, there had been only a single industry-independent study of trace gas emissions from the
56 Athabasca oil sands mining operations (Simpson et al., 2010; Howell et al., 2014). The data showed
57 elevated concentrations in n-alkanes (30% of the total quantified hydrocarbon emissions), cycloalkanes
58 (49%), and aromatics (15%) in plumes from an oil sands surface mining facility intercepted from a single
59 aircraft flight. These compounds are associated with oil and gas developments including mining,
60 upgrading, and transportation of bitumen (Siddique et al., 2006). Specifically, these activities involve the
61 use of naphtha, a complex mixture of aliphatic and aromatic hydrocarbons in the range of C₃ to C₁₄
62 containing n-alkanes (e.g., n-heptane, n-octane, and n-nonane) and benzene, toluene, ethylbenzene,
63 and xylenes (BTEX).

64 In August 2013, a comprehensive air quality study as a part of the Joint Oil Sands Monitoring (JOSM)
65 plan (JOSM, 2012), referred to here as the 2013 JOSM intensive study was conducted. This study was
66 performed in northern Alberta at two ground sites in and near Fort McKay and from a National Research
67 Council of Canada (NRC) Convair 580 research aircraft to characterize oil sands emissions and their
68 downwind physical and chemical transformations (Gordon et al., 2015; Liggio et al., 2016; Li et al., 2017).
69 One ground site, located at the Wood Buffalo Environmental Association (WBEA) air monitoring station

70 (AMS) 13 (Fig. 1), was equipped with a comprehensive set of instrumentation to measure
71 concentrations of trace gases and aerosols (Table 1). As part of this effort, a gas chromatograph
72 equipped with an ion trap mass spectrometer (GC-ITMS) was deployed at AMS 13. When air masses
73 passing over regions with industrial activities were observed (as judged from a combination of local wind
74 direction and tracer measurements), the total ion chromatogram showed an analytically unresolved
75 hydrocarbon signal associated with intermediate volatile organic compounds (IVOCs) with saturation
76 concentration (C^*) in the range $10^5 \mu\text{g m}^{-3} < C^* < 10^7 \mu\text{g m}^{-3}$ (Liggio et al., 2016).

77 Emission estimates for analytically unresolved hydrocarbons range from $5 \times 10^6 \text{ kg year}^{-1}$ to $14 \times 10^6 \text{ kg}$
78 year^{-1} for the two facilities that reported such emissions (Li et al., 2017). Using aircraft measurements
79 during the 2013 study, Liggio et al. (2016) showed that IVOCs contributed to the majority of the
80 observed secondary organic aerosol (SOA) mass production in a similar fashion as anthropogenic VOCs
81 contributed to SOA production during the Deepwater Horizon oil spill (de Gouw et al., 2011) and rivaling
82 the magnitude of SOA formation observed downwind of megacities (Liggio et al., 2016), though
83 ultimately it has remained unclear which activities are associated with IVOC emissions.

84 In this paper, concurrent measurements of air pollutants at the AMS 13 ground site during the 2013
85 JOSM intensive study are presented and analyzed using principal component analysis (PCA) to elucidate
86 the origin of the IVOCs in the Athabasca oil sands. The analysis presented here is a receptor analysis
87 focusing on the normalized variability of pollutants impacting the AMS 13 ground site and hence does
88 not constitute a comprehensive emission profile analysis of the oil sands facilities as a whole, for which
89 aircraft-based measurements and/or direct plume or stack measurements are more suitable. PCA was
90 chosen over the more popular positive matrix factorization (PMF) method (Paatero and Tapper, 1994)
91 because it yields a unique solution and is particularly suited as an exploratory tool for identification of
92 components without *a priori* constraints (Jolliffe and Cadima, 2016). The PCA was complemented by
93 bivariate polar plots (Carslaw and Ropkins, 2012; Carslaw and Beevers, 2013) to show the spatial

94 distribution of sources in the region as a function of locally measured wind direction and speed. A
95 second PCA was performed to investigate which components correlate with (and generate) secondary
96 pollutants, i.e., pollutants that are formed by atmospheric processes. Potential sources and processes
97 contributing to each of the components identified by PCA are discussed.

98

99 **2. Experimental**

100 **2.1 Measurement location**

101 Measurements of air pollutants were made at AMS 13 routine air monitoring station (Fig. 1), which is
102 operated by WBEA. The site is located at 111.6423° W longitude and 57.1492° N latitude about 3 km
103 from the southern edge of the community of Fort McKay, 300 m west from a public road, and 1 km west
104 of the Athabasca river. The immediate vicinity of the site consisted of mixed-leaf boreal forest with a
105 variety of tree species, including poplar, aspen, pine and spruce trees (Smreciu et al., 2013). The site was
106 accessible via a gravel road; traffic on this road was restricted during the study period (August -
107 September, 2013).

108 The site is impacted by emissions from nearby oil sands facilities (Table 1 and Fig. 1), including a large
109 surface mining site operated by Syncrude Canada whose northeastern corner is located 3.5 km to the
110 south of AMS 13 (and which is adjacent to the 5 km long Syncrude – Mildred Lake (SML) tailings pond)
111 and from a large upgrader stack facility operated by Suncor Energy Inc. located to the Southeast. There
112 are additional oil sands facilities operated (during the study period) by Canadian Natural Resources
113 Limited, Imperial Oil, and Shell Canada to the North and Northeast.

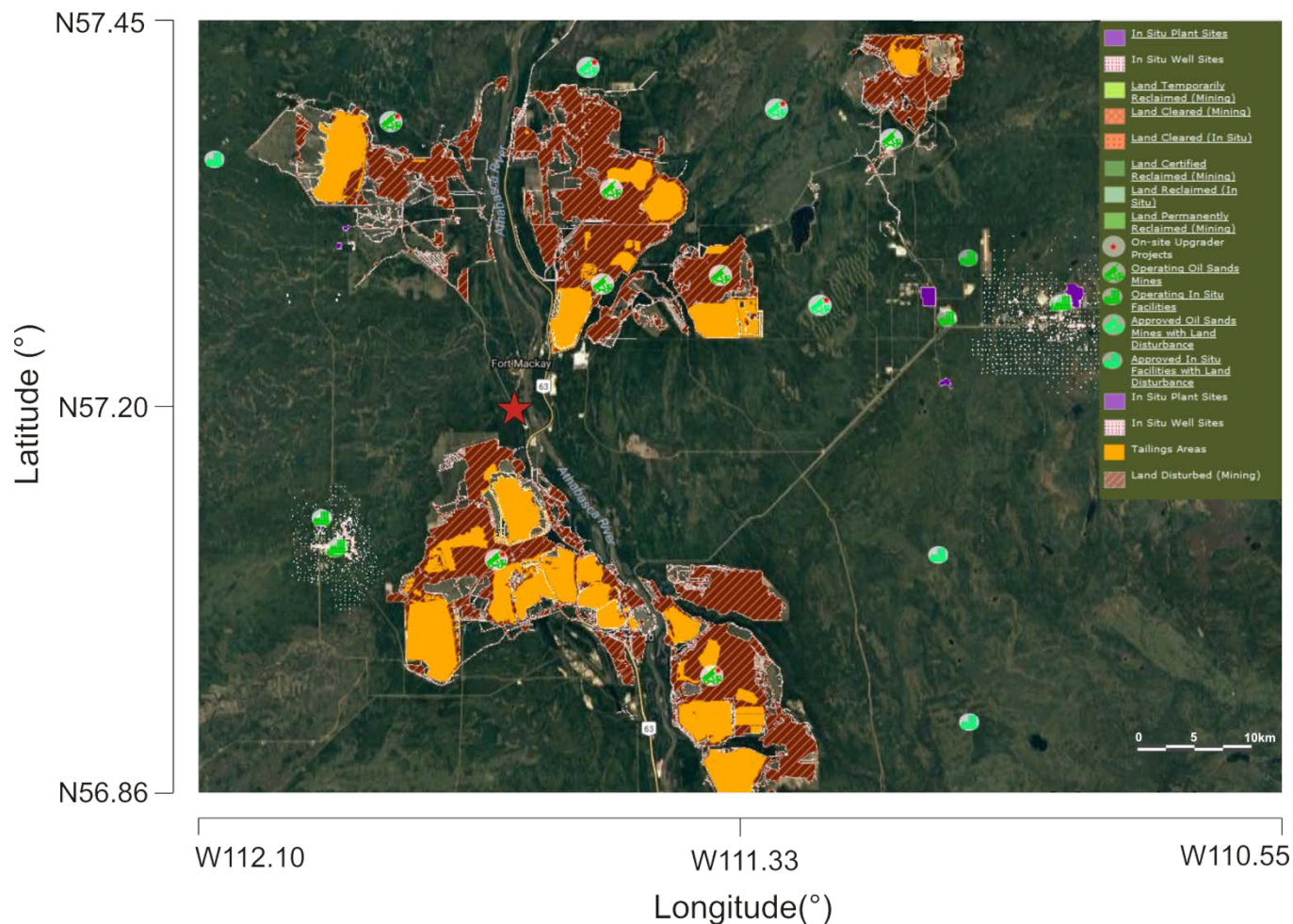
114 **Table 1.** Oil sands facilities located within 30 km of AMS 13. Distances were estimated using coordinates
 115 provided in the National Pollutant Release Inventory (NPRI, 2013) and do not account for the size of
 116 each facility whose boundaries may be considerably closer to (or further away from) AMS 13. PACPRM =
 117 Petroleum and coal products refining and manufacturing; OGPS = Oil and gas pipelines and storage.

Company	Name	Type	Direction	Distance (km)
Syncrude Canada Ltd.	Mildred Lake Plant Site	PACPRM	S	12.2
Athabasca Minerals Inc.	Susan Lake Gravel Pit	Mining and Quarrying	N	15.5
Syncrude Canada Ltd.	Aurora North Mine Site	PACPRM	NE	18.7
Suncor Energy	Suncor Energy Inc. Oil Sands	PACPRM	SE	19.4
Enbridge Pipelines Inc.	Mackay River Terminal	OGPS	WSW	19.7
Suncor Energy	Mackay River, In-Situ, Oil Sands Plant	PACPRM	WSW	19.9
Enbridge Pipelines Inc.	Athabasca Terminal	OGPS	SE	21.2
Williams Energy	Fort McMurray Hydrocarbon Liquids Extraction Facility	Conventional oil and gas extraction	SE	21.6
Canadian Natural Resources Limited	Horizon Oil Sands Processing Plant and Mine	PACPRM	NNW	21.8
Shell Canada Energy	Muskeg River Mine and Jackpine Mine	PACPRM	NNE	23.7

118

119

120 **Figure 1.** Map of oil sands facilities showing locations of surface mines and tailings ponds, downloaded
 121 from the Oil Sands Information Portal (Alberta, 2017). The red star indicates the location of AMS 13.



122

123 **2.2 Instrumentation**

124 A large number of instruments was deployed for this study; a partial list whose data were utilized in this
 125 manuscript is given in Table 2. Detailed descriptions of these instruments and operational aspects such
 126 as calibrations are given in the S.I. Sample observations of analytically unresolved hydrocarbons by GC-
 127 ITMS and how these data were used in the analysis are described in section 2.2.1 below.

128 **Table 2.** Instruments used to measure ambient gas-phase and aerosol species during the 2013 JOSM

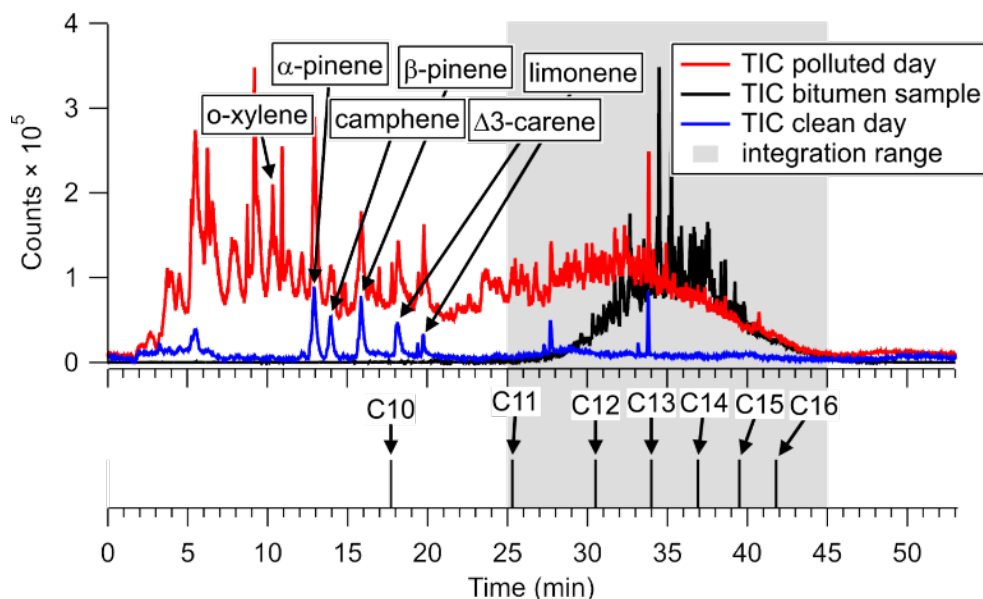
129 intensive study at AMS 13.

Instrument and Model	Species measured	Time resolution	Reference
Picarro CRDS G2401	CO, CO ₂ , CH ₄	1 min	(Chen et al., 2013; Nara et al., 2012)
Thermo Scientific, Model 42i	NO _y	10 s	(Tokarek et al., 2014; Odame-Ankrah, 2015)
Blue diode cavity ring-down spectroscopy	NO ₂	1 s	(Paul and Osthoff, 2010; Odame-Ankrah, 2015)
Thermo Scientific Model 49i	O ₃	10 s	(Tokarek et al., 2014; Odame-Ankrah, 2015)
Griffin/FLIR, model 450 GC-ITMS	VOCs	1 hr	(Tokarek et al., 2017; Liggio et al., 2016)
Thermo Scientific CON101	TS	1 min	n/a
Thermo Scientific 43ITLE	SO ₂	1 min	n/a
AIM-IC	NH _{3(g)} , NH _{4⁺(p)}	1 hr	(Markovic et al., 2012)
Aerodyne SP-AMS	rBC, NH _{4⁺(p)} , SO _{4²⁻(p)} , NO _{3⁻(p)} , Cl ⁻ (p), organics	1-5 min (variable)	(Onasch et al., 2012)
TSI APS 3321	PM ₁₀₋₁ size distribution	5-6 min (variable)	(Peters and Leith, 2003)
TSI SMPS (3081 DMA, 3776 CPC)	PM ₁ size distribution	6 min	(Wang and Flagan, 1990)
EcoChem Analytics PAS 2000CE	pPAH	1 min	(Wilson et al., 1994; Burtscher et al., 1982)

130

131 **2.2.1 Analytically unresolved hydrocarbon signature**

132 As previously reported (Liggio et al., 2016), the total ion chromatogram of the GC-ITMS occasionally
133 showed elevated and analytically unresolved hydrocarbons in the volatility range of C₁₁ – C₁₇ with
134 saturation vapor concentration (C*) from 10⁵ µg m⁻³ < C* < 10⁷ µg m⁻³. An example is shown in Fig. 2.



135
136 **Figure 2. (Top)** Total ion chromatograms of air samples collected on August 27, 2013 from 18:04 to
137 18:14 UTC (red) and on August 28, 2013 from 13:43 to 13:53 UTC (blue). The TIC of a head space sample
138 of ground-up bitumen collected post-campaign is superimposed (black). The gray area indicates the
139 range over which IVOC signal was integrated. **(Bottom)** Retention times of n-alkanes, determined after
140 the measurement intensive by sampling a VOC mixture containing a C₁₀ – C₁₆ n-alkane ladder.

141 An offline analysis of the headspace above ground-up bitumen gave a similarly unresolved hydrocarbon
142 signal (Fig. 2, black trace). In this particular case, the ambient air chromatogram also shows
143 enhancements of lower molecular weight hydrocarbons (possibly from naphtha) that were not observed
144 in the bitumen sample.

145 The major ions contributing to the unresolved signals in Figure 2 are associated with alkanes (i.e., *m/z*

146 55, 57, 67, 69, etc. – see Fig. S-1). In contrast, counts at masses associated with aromatics (i.e., m/z 115,
147 $C_9H_7^+$, and m/z 91, $C_7H_7^+$) as reported by Cross et al. (2013) were negligible in both the bitumen head
148 space and polluted day samples. The strong resemblance of the unresolved hydrocarbon feature in
149 ambient air with the bitumen head space sample both in terms of volatility (i.e., elution time) and
150 electron impact mass fragmentation is consistent with bitumen as the source of IVOCs at this site.

151 In the interpretation of the integrated IVOC signal, it is assumed that it is of primary origin, i.e., emitted
152 directly from point sources in the vicinity of the measurement site. For the PCA analysis, the unresolved
153 signal was integrated from a retention time of 25 min to 45 min (gray area in Fig. 2) in all ambient air
154 chromatograms.

155 The IVOCs observed in this work likely encompass a portion of the total that is emitted. For example,
156 IVOCs generated by combustion processes, such as aircraft engine exhaust, are comprised of alkanes,
157 aromatics and oxygenated compounds (Cross et al., 2013). The use of a chromatographic column in this
158 work biases the IVOC signal towards hydrocarbon-IVOCs, since oxygenated compounds (i.e., alcohols
159 and acids) will not elute from the analytical column. Furthermore, the recovery of VOCs from the pre-
160 concentration unit, while reproducible and likely complete for n-alkanes which bracket the bulk of IVOC
161 emitted and whose calibration curves were linear, is not known for late-eluting compounds, but is
162 assumed to be sufficiently reproducible to yield a semi-quantitative signal.

163

164 **2.3 Principal Component Analysis**

165 The PCA was carried out using the "Statistical Analysis System" (SAS™) Studio 3.4 software (SAS, 2015)
166 using a method similar to that described by Thurston et al. (2011; 1985). The source-related
167 components and their associated profiles are derived from the correlation matrix of the input trace
168 constituents. This approach assumes that the total concentration of each "observable" (i.e., input

169 variable) is made up of the sum of contributions from each of a smaller number of pollution sources and
170 that variables are conserved between the points of emission and observation.

171

172 **2.3.1 Selection of variables**

173 22 variables whose ambient concentrations are dominated by primary emissions or which are formed
174 very shortly after emission (such as the less oxidized oxygenated organic aerosol (LO-OOA) factor
175 observed by the SP-AMS, see below) were included in the PCA (Table 3). These variables included CO₂,
176 CH₄, NO_y, CO, and SO₂, which are known to be emitted in the oil sands region from stacks, the mine fleet
177 and faces, tailings ponds, and by fugitive emissions (Percy, 2013). The median NO_x (= NO + NO₂) to NO_y
178 ratio was 0.85, consistent with the close proximity of the measurement site to emission sources and
179 limited chemical processing. Because NO_x constituted a large fraction of NO_y, its temporal variation was
180 captured by the latter, and it was not included as a separate variable in the PCA analysis.

181 For this work, mixing ratios of all non-methane hydrocarbons (NMHCs) that were quantified (i.e., o-
182 xylene, the n-alkanes decane and undecane, the aromatics 1, 2, 3- and 1, 2, 4-TMB, as well as limonene
183 and α- and β-pinene) were included as variables. In addition, the aforementioned unresolved signal
184 associated with IVOCs was included as a variable by integrating total GC-ITMS ion counts (*m/z* 50–425)
185 over a retention time range of 25–45 min (retention index range of 1100 to 1700).

186 Gas-phase ammonia was included as a variable because elevated reduced nitrogen concentrations have
187 been observed in the region and were linked to the use of ammonia on an industrial scale, for example
188 as a floating agent and for hydrotreating (Bytnerowicz et al., 2010). Total sulfur and total reduced sulfur
189 were added as tracers of upgrader stack SO₂ emissions and of "odours", believed to be emitted from oil
190 sands tailings ponds which continue to be of concern in surrounding communities (Small et al., 2015;
191 Percy, 2013; Holowenko et al., 2000).

192 Refractory black carbon was added as a variable since it is present in diesel truck exhaust and in biomass
193 burning plumes and, hence, a combustion tracer (Wang et al., 2016; Briggs and Long). pPAHs were
194 included because of their association with facility stack emissions and combustion particles in the area
195 (Allen, 2008; Grimmer et al., 1987). Hydrocarbon-like organic aerosol (HOA) was included as a surrogate
196 for fossil fuel combustion by vehicles (Jimenez et al., 2009). The LO-OOA factor was included as it is
197 unique to the Alberta oil sands and appears to form rapidly after emission of precursors (Lee et al.,
198 2018). Supermicron aerosol volume (PM_{10-1} , i.e., the volume of particles between PM_{10} and PM_1) was
199 also included as a tracer of coarse particles from primary sources, which are expected to be dominated
200 by dust emissions.

201

202 **Table 3.** Variables observed at the AMS 13 ground site during the 2013 JOSM campaign used for PCA.

Variable	Unit	Median ^a	Average ^{a,b}	Standard deviation ^{a,b}	LOD ^e	Min. ^a	Max. ^a	Fraction <LOD
<u>Anthropogenic VOCs</u>								
o-xylene	pptv ^f	5	30	69	1	< LOD	635	10%
1,2,3 - TMB	pptv	1.7	4.3	7.9	0.2	< LOD	67	27%
1,2,4 - TMB	pptv	2.1	7.7	14.7	0.2	< LOD	107	8%
decane	pptv	0.5	8.5	18.2	0.1	< LOD	125	44%
undecane	pptv	0.4	3.0	6.3	0.1	< LOD	37	39%
<u>Biogenic VOCs</u>								
α-pinene	pptv	477	542	401	1	19	1916	0%
β-pinene	pptv	390	467	334	1	18	1594	0%
limonene	pptv	150	179	158	2	< LOD	711	1%
<u>Combustion tracers</u>								
NO _y	ppbv	1.79	4.00	5.44	0.01	0.13	41.6	0%
rBC	μg m ⁻³	0.13	0.20	0.10	0.02	< LOD	0.90	40%
CO	ppbv	117.6	120.0	18.2	5.7 ^h	90.9	241.2	0%
CO ₂	ppmv	420.2	433.2	39.5	0.4 ^h	386.0	577.7	0%
<u>Aerosol species</u>								
pPAH	ng m ⁻³	1	2	2	1 ^c	< LOD	14	39%
PM ₁₀₋₁	μm ³ cm ⁻³	11.2	14.4	12.9	0.003	1.0	79.5	0%
HOA	μg m ⁻³	0.31	0.43	0.35	N/A ^g	0.04	2.32	N/A
LO-OOA	μg m ⁻³	1.19	2.00	2.26	N/A ^g	0.11	15.6	N/A
<u>Sulfur species</u>								
Total sulfur (TS)	ppbv	0.22	1.41	4.27	0.13	< LOD	33.3	35%
SO ₂	ppbv	< LOD	1.0	4.0	0.2	< LOD	33.5	81%
Total reduced sulfur (TRS)	ppbv	0.26	0.38	1.05	0.2	< LOD	14.8	81%
<u>Other</u>								
IVOCs	Counts × min	1.8×10 ⁷	3.4×10 ⁷	4.2×10 ⁷	N/A ^g	1.4×10 ⁶	2.5×10 ⁸	N/A
CH ₄	ppbv	1999.2	2065.5	169.6	1.8 ^h	1880	2959	0%
NH ₃	μg m ⁻³	0.79	1.10	1.03	0.05	0.06	5.75	39%

^a Values were determined only from data points included in PCA analysis, not from entire campaign.

^b Average and standard deviation were calculated before zeros were replaced with 0.5×LOD.

^c Estimated.

^e LOD = limit of detection.

^f parts-per-trillion by volume (10⁻¹²)

^g N/A = data not available

^h calculated using 3 × standard deviation at ambient background levels

204 To assess which components have the greatest impact on secondary product formation, a second PCA
 205 was performed which included variables mainly formed through atmospheric chemical processes and
 206 whose concentrations more strongly depend on air mass chemical age than those variables selected
 207 initially. In this PCA, odd oxygen ($O_x = O_3 + NO_2$), submicron aerosol $SO_4^{2-}(p)$, $NO_3^-(p)$, $NH_4^+(p)$, a second,
 208 more-oxidized OOA factor (MO-OOA), and PM_{10} volume were included, increasing the total number of
 209 variables to 28 (Table 4).

210

211 **Table 4.** Variables added in the second PCA. Particle-phase concentrations, i.e., $SO_4^{2-}(p)$, $NO_3^-(p)$, $NH_4^+(p)$
 212 and MO-OOA were made by aerosol mass spectrometry and account for PM_{10} only.

Variable	Unit	Median	Average	Standard deviation	LOD	Min.	Max.
O_x	ppbv	7.35	11.1	10.6	1	<LOD	41.1
$SO_4^{2-}(p)$	$\mu g m^{-3}$	0.3	0.8	1.1	0.1	<LOD	6.6
$NO_3^-(p)$	$\mu g m^{-3}$	0.08	0.13	0.13	0.01	0.01	0.72
$NH_4^+(p)$	$\mu g m^{-3}$	0.13	0.28	0.37	0.05	<LOD	2.21
MO-OOA	$\mu g m^{-3}$	1.65	1.83	0.960	N/A	1.41×10^{-6}	4.65
PM_{10} volume	$\mu m^3 cm^{-3}$	2.48	3.77	3.72	N/A	0.35	20.9

213

214 2.3.2 Treatment of input data

215 Data used in the PCA analysis were averaged to match the time resolution of the GC-ITMS VOC and IVOC
216 measurements, i.e. over 10 minute long periods (spaced ~ 1 hr apart) set by the start and stop times of
217 the GC-ITMS pre-concentration period. When concentrations were below their respective limit of
218 detection (LOD; values are given in Table 3), half the reported LOD was used to minimize bias (Harrison
219 et al., 1996; Buhamra et al., 1998). Prior to PCA, input variables were standardized to eliminate unit
220 differences by subtracting the mean concentration \bar{C}_i of pollutant i from the concentration of sample k
221 ($C_{i,k}$) and dividing by the standard deviation (s_i) of all samples included in the PCA analysis.

$$222 \quad Z_{i,k} = \frac{C_{i,k} - \bar{C}_i}{s_i} \quad (1)$$

223 Here, $Z_{i,k}$ is the standardized pollutant concentration. In total, 218 data points from all identified species
224 over the period of the campaign were used for the main PCA analysis.

225

226 2.3.3 PCA solutions

227 In this work, the Varimax method (Kaiser, 1958) was used to rotate the loading matrix. This method is an
228 orthogonal rotation (i.e., components are not expected to correlate) which minimizes the impact of high
229 loadings, making the results easier to interpret (Kaiser, 1958). Several criteria (Table S-10) were
230 considered for component selection: the latent root criterion, i.e., on the basis that rotated eigenvalues
231 must be greater than unity, the (cumulative) percentage of variance criterion, where the extracted
232 components accounts for >95% of the variance, and the Scree test (Fig. S-2) (Thurston and Spengler,
233 1985; Guo et al., 2004; Hair et al., 1998; Cattell, 1966). For the optimal solution presented in the main
234 manuscript, the 95% variance criterion was chosen, providing a 10-component solution for the PCA with

235 only primary variables and an 11-component solution for the PCA with both primary and secondary
236 variables. Components 1 through 4 were consistent regardless of the number of components retained.
237 Solutions with fewer and more components are presented in the supplemental material section.
238 Time series of each of the components were calculated by multiplying the original standardized matrix
239 by the rotated loading matrix and were used to generate bivariate polar plots (section 2.4).

240

241 **2.4 Bivariate polar plots**

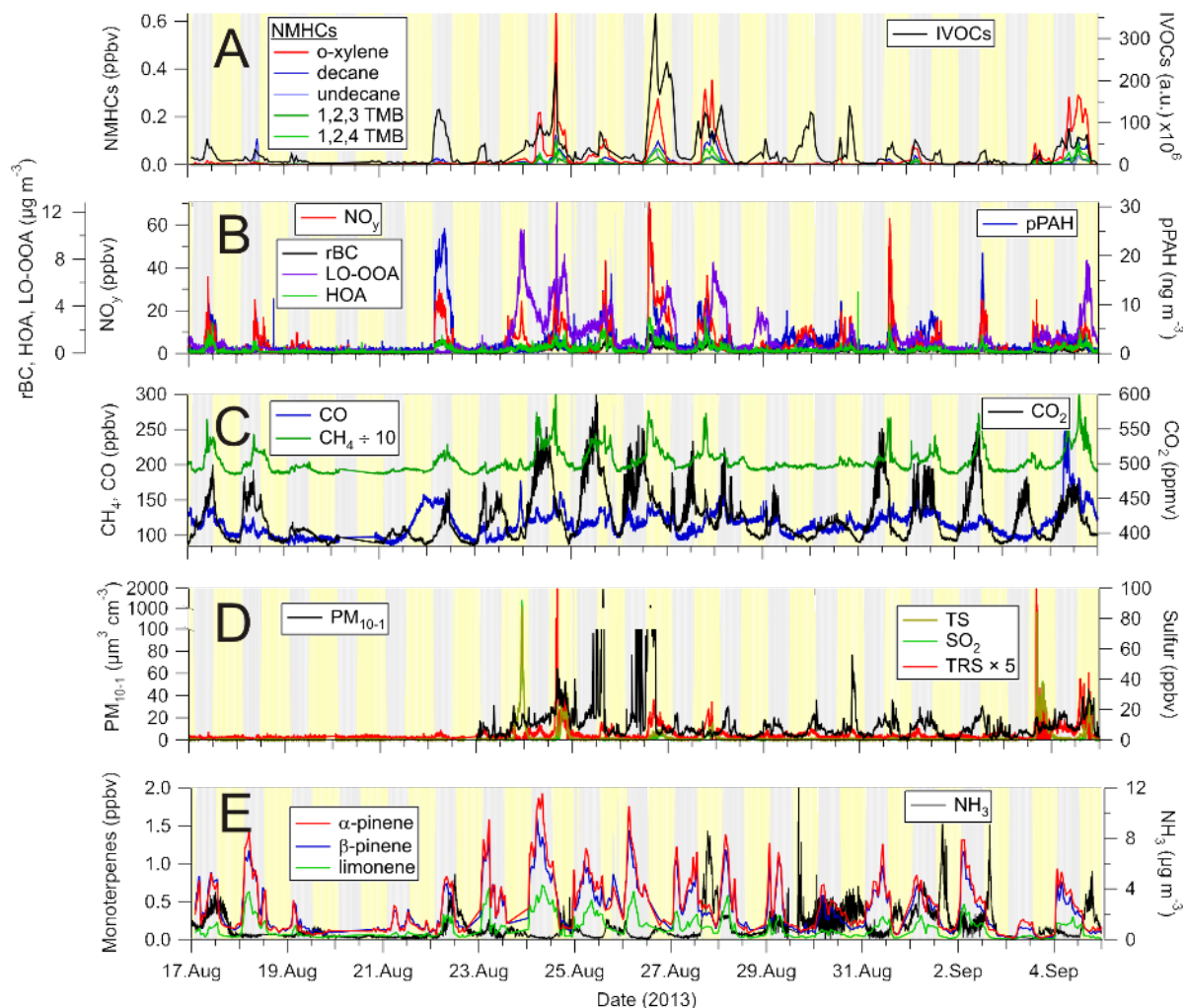
242 The PCA was complemented by bivariate polar plots showing the wind speed and direction dependence
243 of air pollutant concentrations. The use of these representations implies a linear relationship between
244 local wind conditions and air mass origin, which may not be always the case (for example, during or after
245 stagnation periods). In addition, local topography, such as the Athabasca river valley, complicates
246 regional air flow patterns and limit the interpretability of polar plots in general and in particular to the E
247 of AMS 13, where the river valley is located. The plots were generated with the Openair software
248 package (Carslaw and Ropkins, 2012; Carslaw and Beevers, 2013) using the R programming language and
249 the open-source software "RStudio: Integrated development environment for R" (RStudio Boston,
250 2017). The default setting (100) was used as the smoothing function.

251 **3. Results**

252 **3.1. Overview of the data set**

253 Time series of the 22 pollution tracers chosen for PCA analysis are presented in Fig. 2, grouped
254 approximately by source type. Statistics of the data (i.e., median, average, maxima, minima, etc.) are
255 summarized in Table 3.

256



257

258 **Figure 3.** Time series of selected pollution tracers observed at the AMS 13 ground site in the Athabasca
 259 oil sands during the 2013 JOSM measurement intensive. The gray and yellow backgrounds represent
 260 night and day, respectively. **(A)** Selected non-methane hydrocarbons (NMHCs) and IVOCs. **(B)**
 261 Combustion product tracers: refractory black carbon (rBC), total odd nitrogen (NO_y) and particle surface
 262 bound polycyclic aromatic hydrocarbons (pPAH), and organic aerosol components: hydrocarbon-like
 263 organic aerosol (HOA) and less oxidized oxygenated organic aerosol (LO-OOA). **(C)** Methane (CH_4),
 264 carbon dioxide (CO_2) and monoxide (CO). **(D)** Total sulfur (TS), sulfur dioxide (SO_2), and total reduced
 265 sulfur (TRS) and PM_{10-1} particle volume. **(E)** Biogenic VOCs (α -pinene, β -pinene and limonene) and
 266 ammonia (NH_3).

267 Time series of VOCs of primarily anthropogenic origin (i.e., o-xylene, 1, 2, 3- and 1, 2, 4-TMB, etc.) as
268 well as the IVOC signature are shown in Fig. 3A. The abundances of these species, as well as the other
269 compounds, were highly variable and varied as a function of time of day (i.e., boundary layer mixing
270 height) and air mass origin, with higher VOC concentrations generally observed during daytime. The VOC
271 concentrations varied between nearly pristine, remote conditions, with concentrations below
272 detectable limits, to mixing ratios of aromatic species exceeding 100 pptv. The concentration range of o-
273 xylene is within the extremes reported by WBEA in their 2013 annual report (WBEA, 2013), exemplifying
274 that the data set is representative of typical pollutant levels in this region.

275 While there is some obvious covariance between variables (i.e., when the mixing ratios of one particular
276 VOC increases, so do others), the ratios of hydrocarbons varied considerably. For example, on August
277 18, 10:50 UTC, the n-decane to o-xylene ratio was ~22:1, whereas on August 24, 07:40 UTC it was ~1:5.7.
278 The IVOC magnitude also varied greatly and often increased and decreased in tandem with the other
279 VOCs (e.g., on Aug 24, 16:30 UTC) but also increased independently from the other VOC abundances
280 (e.g., on Aug 30, 01:20 UTC, and on the night of Aug 22). This behaviour suggests the presence of
281 multiple sources with distinct signatures that are being sampled to a varying extent at different times.
282 This, coupled with the intermittency of the highly elevated signals, presents an analysis problem
283 frequently encountered in environmental analysis that is usually investigated through a factor or
284 principal component analysis (Thurston et al., 2011; Guo et al., 2004).

285 Presented in Fig. 3B are the time series of NO_y, rBC and pPAH abundances, all of which are combustion
286 byproducts. For example, rBC is emitted from combustion of fossil fuels, biofuels, open biomass burning,
287 and burning of urban waste (Bond et al., 2004). Similar to the VOCs, the abundances of these species
288 varied greatly, from very low, continental background levels (i.e., <100 pptv of NO_y, < LOD for rBC and
289 pPAHs) to polluted concentrations (i.e., > 60 ppbv of NO_y, > 1 μg m⁻³ rBC, > 10 ng m⁻³ pPAHs)
290 characteristic of polluted urban and industrial areas. When high concentrations of NO_y were observed,

291 its main component was NO_x (data not shown), which is a combustion byproduct usually associated with
292 automobile exhaust. In the Alberta oil sands, emissions from off-road mining trucks as well as the
293 upgrading processes are the main contributors to the NO_y burden (Percy, 2013; Watson et al., 2013).
294 Shown in Fig. 3C are the mixing ratios of the greenhouse gases CH₄ and CO₂ along with CO. Abundances
295 of CO₂ were clearly attenuated by photosynthesis and respiration of the vegetation near the
296 measurement site, as judged from the strong diurnal cycle in its concentration (not shown). Maxima
297 typically occurred shortly after sunrise, coincident with the expected break-up of the nocturnal
298 boundary layer. In addition to biogenic emissions from vegetation and soil, CO₂ originates from a variety
299 of point and mobile sources in this region, including off-road mining trucks (Watson et al., 2013) and the
300 extraction, upgrading, and refining of bitumen and on-road vehicle sources in the area (Nimana et al.,
301 2015a, b). Concentrations of CO₂ spiked whenever these emissions were transported to the
302 measurement site.

303 Concentrations of CH₄ also exhibit a diurnal cycle, with higher concentrations generally observed at
304 night and peaking in the early morning hours. While CH₄ and CO₂ mixing ratios frequently correlated in
305 plumes, their ratios were variable overall, suggesting they often originated from distinct sources.
306 Potential methane point sources in the region include microbial production in tailings ponds (Siddique et
307 al., 2012) and fugitive emissions associated with the mining and processing of bitumen (Johnson et al.,
308 2016). Indeed, a recent analysis shows tailings ponds and open pit mining sources to be the largest
309 sources of CH₄ in the region (Baray et al., 2018).

310 Similar to the anthropogenic VOCs, the abundances of CH₄ and CO₂ were highly variable and ranged
311 from minima of 1.88 and 384 ppmv to maxima of 2.96 and 578 ppmv, corresponding to maximum
312 enhancements of 1.63 and 1.47 relative to tropospheric global monthly means of 1.806±0.001 and
313 394.3±0.1 ppmv for July, 2013 (Dlugokencky, 2017b, a), respectively.

314 Mixing ratios of CO also varied with time but generally were not elevated greatly (median 118 ppbv)
315 above background levels (minimum 91 ppbv), except for occasional spikes in concentration (Fig. 3C).
316 Carbon monoxide is a tracer of biomass burning and fossil fuel combustion, in particular in automobiles
317 with poorly performing or absent catalytic converters, but is also a byproduct of the oxidation of VOCs,
318 in particular of methane and isoprene which are oxidized over a wide area upwind of AMS 13 (Miller et
319 al., 2008).

320 Time series of sulfur species and PM₁₀₋₁ volume are shown in Fig. 3D. The TS and SO₂ data are dominated
321 by intermittent plumes containing SO₂ mixing ratios exceeding 5 ppbv. The highest mixing ratio
322 observed was 92.5 ppbv (in between the preconcentration periods of the GC-ITMS). Mixing ratios of SO₂
323 exhibited the most variability of all pollutants, as judged from the standard deviation of each of the
324 measurements (Table 3). TRS levels were generally small (< 1 ppbv) and variable, except for plumes; TRS
325 abundances in plumes, however, are more uncertain since they were calculated by subtraction of two
326 large numbers. When TS and SO₂ abundances were low (< 1 ppbv), TRS abundances were variable and
327 occasionally exhibited spikes that did not show any obvious correlation with other variables, suggesting
328 the presence of one or more distinct TRS sources. PM₁₀ volume concentrations varied a lot as well and,
329 just like TRS, did not show an obvious correlation with other variables. Fugitive dust emissions likely
330 contributed to much of the PM₁₀ volume in the Athabasca oil sands region (Wang et al., 2015).

331 Time series of monoterpene mixing ratios are shown in Fig. 3E. α -Pinene was generally the most
332 abundant monoterpene, followed by β -pinene. Their ratio, averaged over the entire campaign was
333 1:0.85, though occasionally the α - to β -pinene ratio was below 1:2 (e.g., on Aug 28, 14:50 UTC and Sept
334 5, 12:40 UTC). Terpene mixing ratios were generally higher at night than during the day, with maxima of
335 1.9 and 1.6 ppbv, respectively, a diurnal pattern consistent with what has been observed at other forest
336 locations (Fuentes et al., 1996). Monoterpenes are emitted by plants via both photosynthetic and non-
337 photosynthetic pathways (Fares et al., 2013; Guenther et al., 2012); at night, their emissions accumulate

338 in a shallow nocturnal boundary layer, whereas during daytime, they are entrained aloft (above the
339 canopy) and oxidized by the hydroxyl radical (OH) and O₃, which are more abundant during the day than
340 at night (Fuentes et al., 1996). α- and β-pinene mixing ratios were lowest mid-day (median values at
341 noon of 140 and 133 pptv, respectively). The largest daytime concentrations were observed on Aug 25, a
342 cloudy day (as judged from spectral radiometer measurements of the NO₂ photolysis frequency): on this
343 particular day, mixing ratios at noon were 687 and 850 pptv, respectively.

344 Also shown in Fig. 3E is the time series of ammonia. These data were dominated by spikes which were
345 observed sporadically and did not correlate with other variables, suggesting the presence of nearby
346 ammonia point sources. Ammonia was not as variable as some of the other pollutants (e.g., the
347 anthropogenic VOCs, sulfur species) as judged from its standard deviation (Table 3), which suggests a
348 geographically more disperse source or sources similar to CO or CH₄, which have a "background". This is
349 consistent with a recent study by Whaley et al. (2017) that estimated over half (~57%) of the near-
350 surface NH₃ during the study period originated from NH₃ bi-directional exchange (i.e. re-emission of NH₃
351 from plants and soils), with the remainder being from a mix of anthropogenic sources (~20%) and forest
352 fires (~23%).

353

354 **3.2. Principal component analysis**

355 **3.2.1. PCA analysis with primary variables**

356 The loadings of the optimum solution are presented in Table 5. The 10-component solution accounts for
357 a cumulative variance of 95.5%. The communalities for the analysis, i.e., the fraction of total pollutant
358 observations accounted for by the PCA are all greater than 85%, with the lowest communality obtained
359 for the IVOCs (0.86).

360 In the following, an overview of the observed components is presented. Associations with $r > 0.7$, $r > 0.3$,

361 and $r > 0.1$ are referred to as "strong", "weak", and "poor", respectively. Hypothesized identifications are
362 given in section 4 and are summarized in Table 6 and Fig. 4.

363 The component accounting for most of the variance of the data, component 1, is strongly associated
364 with the anthropogenic VOCs ($r > 0.87$), weakly associated with CH_4 ($r = 0.59$), TRS ($r = 0.59$), HOA ($r =$
365 0.40), LO-OOA ($r = 0.45$), CO ($r = 0.41$), and the IVOCs ($r = 0.31$), and poorly associated with NO_y ($r =$
366 0.27) and rBC ($r = 0.30$). Component 2 is strongly associated with the combustion tracers NO_y ($r = 0.82$),
367 rBC ($r = 0.77$), HOA ($r = 0.74$), and pPAH ($r = 0.94$), weakly associated with CH_4 ($r = 0.39$) and IVOCs ($r =$
368 0.39), and poorly associated with ammonia ($r = 0.20$), CO ($r = 0.18$) and undecane and decane ($r = 0.27$
369 and 0.22 , respectively). Component 3 is strongly associated ($r > 0.9$) with the biogenic VOCs and weakly
370 associated with CO_2 ($r = 0.48$) and shows poor negative correlations with NO_y ($r = -0.26$), ammonia ($r = -$
371 0.24), and SO_2 ($r = -0.15$). Component 4 is strongly associated with SO_2 and TS ($r = 0.97$ and 0.93 ,
372 respectively) and poorly with NO_y ($r = 0.21$) and LO-OOA ($r = 0.28$).

373 Components 1 through 4 emerged regardless of the number of components used to represent the data,
374 whereas the structure of components 5 through 10 only fully emerged in the 10-component solution
375 (see S.I.). Hence, components 6 through 10 are somewhat tentative as many (i.e., 7 – 9) are single
376 variable components and have eigenvalues close to or below unity, i.e., account for less variance than
377 any single variable. As a result, the interpretations of these components are subject to more uncertainty
378 and are more speculative but are presented in the S.I. for the sake of completeness and transparency.
379 For the purpose of this manuscript, this is inconsequential as components 6 – 10 are not associated with
380 IVOCs.

381

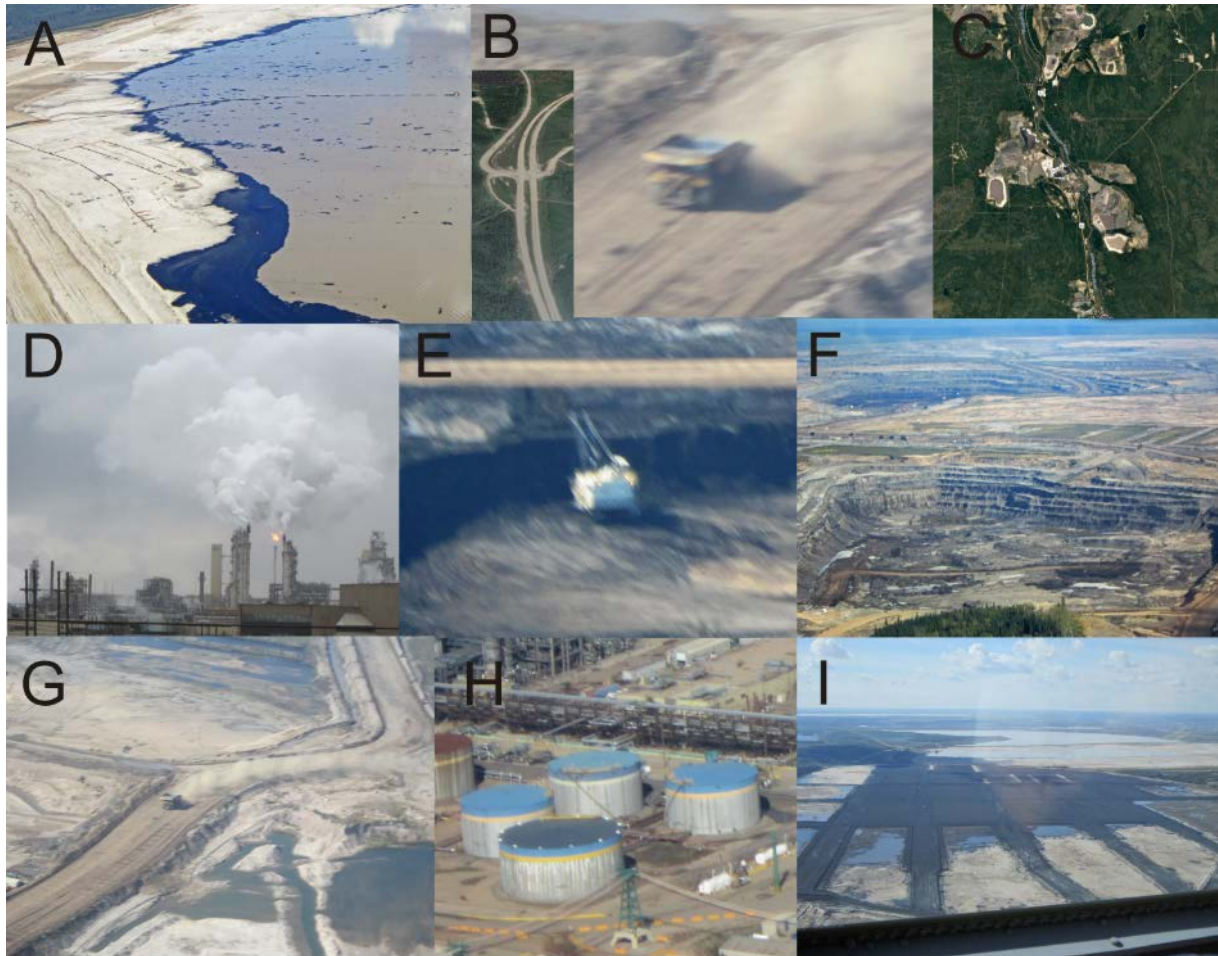
382 **Table 5.** Loadings for the 10-factor, optimal solution (primary variables only). Coefficients with Pearson
 383 correlation coefficients $r > 0.3$ are shown in bold font.

	1	2	3	4	5	6	7	8	9	10	Communalities
Anthropogenic VOCs											
o-xylene	0.88	0.08	0.02	0.10	0.14	0.13	0.07	-0.04	0.16	0.32	0.95
1,2,3 - TMB	0.93	0.16	0.07	0.05	0.05	0.11	0.04	-0.02	0.18	-0.01	0.95
1,2,4 - TMB	0.94	0.14	0.01	0.10	0.11	0.08	0.07	-0.03	0.18	0.13	0.98
decane	0.92	0.22	-0.02	0.15	0.23	0.01	0.05	0.04	0.04	0.03	0.97
undecane	0.87	0.27	-0.08	0.23	0.20	-0.06	0.12	0.07	-0.04	-0.10	0.96
Biogenic VOCs											
α -pinene	-0.03	-0.08	0.98	-0.11	0.02	0.04	0.01	-0.08	0.02	0.01	0.98
β -pinene	-0.02	-0.08	0.98	-0.12	0.02	0.03	0.02	-0.07	0.00	0.01	0.98
limonene	0.07	-0.03	0.92	-0.08	0.12	0.24	0.05	-0.11	0.03	-0.05	0.95
Combustion tracers											
NO _y	0.27	0.82	-0.26	0.21	0.22	-0.04	0.02	0.10	-0.08	0.01	0.92
rBC	0.30	0.77	0.03	0.05	0.44	0.10	0.09	0.13	0.12	-0.10	0.94
CO	0.41	0.18	0.04	0.02	0.09	0.09	0.08	0.06	0.87	-0.01	0.99
CO ₂	0.09	0.08	0.48	-0.12	-0.03	0.77	0.25	-0.14	0.05	-0.08	0.95
Aerosol species											
pPAH	0.06	0.94	-0.07	-0.13	-0.11	0.07	0.01	0.13	0.10	0.04	0.95
PM ₁₀₋₁	0.18	0.14	0.08	0.09	0.11	0.17	0.93	-0.03	0.07	0.08	0.98
HOA	0.40	0.74	0.02	0.12	0.25	0.15	0.23	-0.06	0.16	0.09	0.90
LO-OOA	0.45	0.11	0.12	0.28	0.72	0.05	0.25	0.00	0.10	0.04	0.91
Sulfur											
TS	0.25	0.04	-0.16	0.93	0.08	-0.05	0.07	-0.02	0.01	0.12	1.00
SO ₂	0.12	0.03	-0.15	0.97	0.02	-0.04	0.03	-0.03	0.01	-0.05	0.99
TRS	0.59	0.04	-0.08	0.11	0.26	-0.04	0.16	0.04	-0.04	0.71	0.96
Other											
IVOCs	0.31	0.39	0.12	-0.08	0.74	-0.02	-0.02	-0.06	0.02	0.20	0.86
NH ₃	0.01	0.20	-0.24	-0.05	-0.02	-0.08	-0.03	0.94	0.04	0.02	0.99
CH ₄	0.59	0.39	0.10	-0.05	0.12	0.59	0.11	0.00	0.17	0.14	0.93
Eigenvalues	5.72	3.32	3.23	2.16	1.64	1.13	1.13	0.99	0.96	0.74	
% of variance	25.99	15.08	14.69	9.80	7.46	5.14	5.13	4.51	4.36	3.35	
Cumulative variance	25.99	41.07	55.76	65.56	73.02	78.16	83.30	87.81	92.17	95.52	

384

385 **Table 6.** Hypothesized identifications of principal components.

Component	Key observations	Possible source(s)	Relevant references
1	Enhancements of aromatics, n-alkanes, TRS, NO _y , rBC, HOA, LO-OOA, CO and CH ₄	Wet tailings ponds and associated facilities	(Simpson et al., 2010; Small et al., 2015; Percy, 2013; Holowenko et al., 2000; Howell et al., 2014)
2	Enhancements of NO _y , rBC, pPAH and HOA due to engine exhaust	Mine fleet and operations	(Wang et al., 2016; Grimmer et al., 1987; Allen, 2008; Briggs and Long, 2016)
3	Enhancements of monoterpenes and CO ₂ , poor anticorrelation with NO _y and absence of anthropogenic VOCs	Biogenic emission and respiration	(Guenther et al., 2012; Helmig et al., 1999)
4	Enhancements of SO ₂ and TS, poor correlation with NO _y and LO-OOA	Upgrader facilities	(Simpson et al., 2010; Kindziarski and Ranganathan, 2006)
5	Enhancements of IVOCs, rBC, LO-OOA, NO _y , and TRS	Surface exposed bitumen and hot-water based bitumen extraction	this work
6	Enhancements of CO ₂ and CH ₄ , absence of combustion tracers	Mine face and soil	(Johnson et al., 2016; Rooney et al., 2012)
7	Enhancement of PM ₁₀₋₁	Wind-blown dust	(Wang et al., 2015)
8	Enhancement of ammonia	Fugitive emissions from storage tanks and natural soil/plant emissions	(Bytnerowicz et al., 2010; Whaley et al., 2017)
9	Enhancement of CO	Incomplete hydrocarbon oxidation	(Marey et al., 2015)
10	Enhancements of TRS and o-xylene, poor association with CH ₄	Composite tailings	(Small et al., 2015; Warren et al., 2016)



387

388 **Figure 4.** Images of likely sources associated with each of the principal components. From top left to
 389 bottom: **(A)** Wet tailings ponds (component 1). **(B)** Mine truck fleet and highway traffic emissions
 390 (component 2). **(C)** Biogenic emissions from vegetation (component 3). **(D)** Upgrader facilities
 391 (component 4). **(E)** Exposed bitumen on mined surfaces (component 5). **(F)** Fugitive greenhouse gas
 392 emissions from mine faces (component 6). **(G)** Wind-blown dust from exposed sand (component 7). **(H)**
 393 Fugitive emissions of ammonia from storage tanks (Component 8). **(I)** Composite (dry) tailings
 394 (component 10). No image is shown for production CO from oxidation of VOCs (component 9).

395

396 3.2.2. Extended PCA analysis with added secondary variables

397 The loadings of the optimum solution that includes primary and secondary variables are shown in Table
398 7. In this 11-component solution, the 10 components originally identified were preserved, though their
399 relative order was changed, with the upgrader component moving from the 4th to 2nd position. There
400 was one new component (#6), which encompassed only secondary species, including MO-OOA ($r =$
401 0.92), O_x ($r = 0.33$), $NO_3^-_{(p)}$ ($r = 0.36$), PM_1 ($r = 0.31$) and LO-OOA ($r = 0.31$).

402 $NH_4^+_{(p)}$, $SO_4^{2-}_{(p)}$, and $NO_3^-_{(p)}$ are associated with the stack emissions component (#2, with $r = 0.84$, 0.84
403 and 0.44 , respectively), which also weakly correlated with PM_1 ($r = 0.44$) and O_x ($r = 0.36$). The
404 association of secondary variables with the primary components suggests rapid formation of these
405 secondary products on a time scale that is similar to the transit time of the pollutants to the
406 measurement site. PM_1 correlated strongly with the major IVOC component (component 5, $r = 0.80$),
407 which also weakly associated with LO-OOA ($r=0.66$) and $NO_3^-_{(p)}$ ($r = 0.59$), as well as $NH_4^+_{(p)}$ and $SO_4^{2-}_{(p)}$ (r
408 $= 0.32$ and 0.33 , respectively).

409

410 **Table 7.** Loadings for the 11-component solution with the inclusion of variables associated with

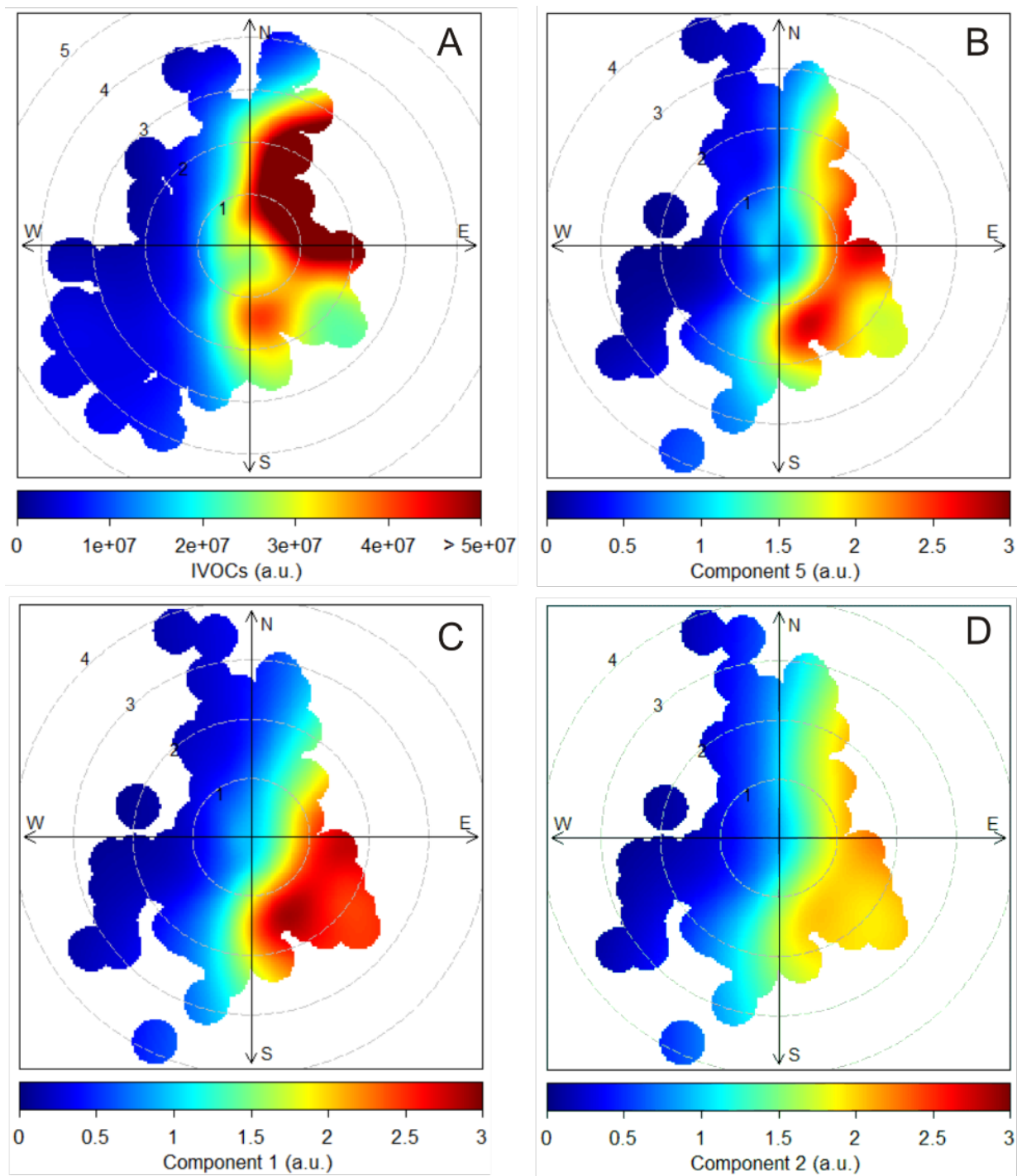
411 secondary processes.

	1	2	3	4	5	6	7	8	9	10	11	Communalities
Anthropogenic VOCs												
o-xylene	0.89	0.16	0.04	0.04	0.15	0.00	0.10	0.07	-0.04	0.17	0.24	0.94
1,2,3 - TMB	0.91	0.13	0.10	0.16	0.09	0.07	0.11	0.03	-0.03	0.16	-0.08	0.95
1,2,4 - TMB	0.93	0.19	0.02	0.13	0.13	0.05	0.06	0.07	-0.03	0.17	0.06	0.99
decane	0.89	0.25	0.00	0.22	0.26	0.05	-0.01	0.05	0.01	0.00	0.01	0.98
undecane	0.81	0.35	-0.08	0.27	0.21	0.15	-0.07	0.08	0.04	-0.12	-0.10	0.96
Biogenic VOCs												
α-pinene	0.00	-0.08	0.98	-0.07	0.05	0.03	0.01	0.01	-0.07	0.02	0.01	0.98
β-pinene	0.01	-0.08	0.98	-0.08	0.05	0.05	0.01	0.03	-0.06	0.01	0.02	0.98
limonene	0.11	-0.02	0.92	-0.02	0.14	0.09	0.21	0.02	-0.10	0.02	-0.03	0.95
Combustion tracers												
NO _y	0.23	0.20	-0.27	0.82	0.21	-0.06	-0.07	0.03	0.10	-0.10	0.01	0.92
rBC	0.22	0.15	0.05	0.80	0.43	0.15	0.10	0.05	0.09	0.07	0.00	0.95
CO	0.40	0.09	0.08	0.20	0.09	0.22	0.08	0.06	0.03	0.83	-0.02	0.97
CO ₂	0.12	-0.07	0.50	0.08	-0.03	0.09	0.75	0.28	-0.12	0.03	-0.08	0.95
Aerosol species												
pPAH	0.06	-0.10	-0.06	0.93	-0.07	-0.06	0.07	0.03	0.15	0.13	-0.05	0.94
PM ₁₀₋₁	0.19	0.16	0.08	0.16	0.13	0.08	0.18	0.91	-0.03	0.05	0.07	0.99
PM ₁	0.24	0.44	0.00	0.17	0.70	0.31	-0.06	0.11	-0.04	0.07	-0.14	0.90
NH ₄ ⁺ (p)	0.28	0.84	0.02	0.12	0.32	0.22	0.06	0.07	-0.04	0.14	-0.04	0.97
SO ₄ ²⁻ (p)	0.29	0.84	0.03	0.12	0.33	0.19	0.06	0.06	-0.05	0.12	-0.05	0.97
NO ₃ ⁻ (p)	0.30	0.44	0.09	0.23	0.59	0.36	0.08	0.15	-0.13	0.02	0.24	0.92
HOA	0.37	0.18	0.02	0.77	0.25	0.10	0.10	0.18	-0.08	0.13	0.14	0.93
LO-OOA	0.37	0.40	0.12	0.16	0.66	0.31	0.03	0.12	-0.06	0.00	0.27	0.97
MO-OOA	0.10	0.15	0.09	0.00	0.10	0.92	0.05	0.07	0.10	0.16	-0.03	0.95
Sulfur												
TS	0.27	0.90	-0.20	0.03	0.04	-0.04	-0.09	0.07	0.00	-0.04	0.18	0.98
SO ₂	0.09	0.96	-0.19	0.02	-0.03	-0.01	-0.08	0.03	-0.02	-0.03	0.00	0.98
TRS	0.65	0.14	-0.10	0.05	0.23	-0.08	-0.07	0.17	0.06	-0.04	0.63	0.95
Other												
IVOCs	0.34	-0.01	0.12	0.33	0.80	-0.23	-0.02	0.02	0.02	0.06	0.06	0.94
NH ₃	-0.03	-0.08	-0.22	0.21	-0.04	0.09	-0.07	-0.03	0.93	0.02	0.02	0.99
O _x	0.07	0.36	-0.62	0.01	0.27	0.33	-0.41	-0.07	-0.03	-0.14	0.12	0.91
CH ₄	0.60	0.00	0.14	0.42	0.10	0.08	0.57	0.08	-0.04	0.13	0.16	0.94
Eigenvalues	5.85	4.30	3.71	3.51	2.78	1.58	1.24	1.09	1.01	0.94	0.75	
% of variance	20.90	15.34	13.25	12.52	9.92	5.65	4.43	3.88	3.59	3.37	2.66	
Cumulative variance	20.90	36.24	49.49	62.02	71.94	77.59	82.03	85.90	89.50	92.87	95.53	

412 **3.3 Spatial distribution of IVOC sources**

413 Bivariate polar plots were generated for all components and their dominant, associated variables and
414 are shown in the supplemental material section (Figs. S2-S11). Winds were predominantly from the SW
415 but were also observed often from the S and N. Fig. 5A shows the plot for IVOCs. The highest
416 concentrations were observed when the local wind direction was from the NE, where several facilities
417 including the Aurora North, Musket River and Jackpine mines and large swaths of disturbed and cleared
418 land are located in close proximity to each other (Table 1 and Fig. 1). The second highest IVOC signal
419 intensity was observed when local wind direction was from the SSE.

420 The bivariate polar plots of the 3 components associated with IVOCs are shown in Fig. 5B-D. These
421 components are associated with winds from the NE, E, SE and S at low to moderate speeds ($1-3 \text{ m s}^{-1}$).
422 Component 5 (Fig. 5B) was the most strongly correlated with IVOCs and shows the most spatial overlap
423 with the distribution of the IVOC source; however, the intensities differ owing to the association of
424 component 5 with other variables such rBC and LO-OOA.



425

426 **Figure 5.** Bivariate polar plots related to IVOCs: **(A)** IVOCs from the complete data set. **(B)** Component 5
 427 extracted from the main PCA (Table 5). **(C)** Component 1 extracted from the main PCA. **(D)** Component 2
 428 extracted from the main PCA analysis. Wind direction is binned into 10° intervals and wind direction into
 429 30° intervals. The polar axis indicates wind speed (m s^{-1}). a.u. = arbitrary units.

430 4. Discussion

431 The main objective of this work is to elucidate the origin of the IVOC signature observed at the AMS 13
432 ground site downwind from the AB oil sands mining operations (Fig. 2) through a principal component
433 analysis. The optimum PCA solution identified 10 components, of which three were associated with the
434 IVOC signature: 1, 2, and 5 (Table 5). The assignments of these components to source types in the oil
435 sands are given in Table 6 and are discussed below.

436 Emission inventories show that the facilities that process the mined bitumen are by far the largest
437 anthropogenic point sources in the oil sands region (NPRI, 2013), consistent with recent aircraft
438 measurements (Baray et al., 2018; Howell et al., 2014; Li et al., 2017; Simpson et al., 2010) which have
439 shown substantial emissions of NO_y, SO₂, CO, VOCs, CO₂, and CH₄, from these facilities and associated
440 mining activities. No single component correlates with all of these variables, suggesting that the PCA is
441 able to distinguish between source types within the facilities such as tailings ponds (component 1), stack
442 emissions (component 4), and mining (component 2).

443 Close-up overflights (Howell et al., 2014; Li et al., 2017; Baray et al., 2018) were able to spatially resolve
444 various oil sands facility emission sources (i.e., tailings ponds from upgraders, fluid coking reactors,
445 hydrocrackers and –treaters); the PCA presented in this manuscript is not expected to do this in all cases
446 because some emissions would have frequently merged into a single plume by the time of observation
447 at AMS 13; unless their emissions vary considerably in time, these sources could be interpreted as
448 originating from a single source in the PCA.

449 The discussion below focuses on components that are associated with IVOCs (section 4.1), followed by
450 those that are not (section 4.2). The PCA analysis that included 6 secondary products is discussed in
451 section 4.3. Components which are not associated with IVOCs and have only tentatively been identified
452 (i.e., components 6 – 10) are discussed in the S.I.

453 4.1 Sources associated with IVOCs

454 4.1.1. Component 1: Tailings ponds (wet tailings)

455 Component 1 is strongly associated with anthropogenic VOCs ($r > 0.87$) and weakly with TRS ($r = 0.59$),
456 and CH_4 ($r = 0.59$). These pollutants originate from tailings ponds (Small et al., 2015), though it is unclear
457 from this analysis how large a source tailings ponds are compared to fugitive emissions of these
458 pollutants from the nearby processing (e.g., bitumen separation and mining) facilities.

459 Tailings ponds cover large areas of land and are used to slowly (on a time scale of years to decades)
460 separate solid components, or tailings, from water used in bitumen extraction. Residual bitumen often
461 floats to the top of the settling basins. Most tailings ponds are "wet" (as they contain residual naphtha
462 that is used as a diluent during the transfer of tailings to the ponds) and emit VOCs, CH_4 , and CO_2 (Small
463 et al., 2015). The presence of o-xylene, TMB and the n-alkanes in component 1 is consistent with the
464 fugitive release of VOCs from residual naphtha, which contains these compounds (Siddique et al., 2008;
465 Siddique et al., 2011; Small et al., 2015). Furthermore, the observation of TRS and CH_4 from this source is
466 consistent with the presence of anaerobic sulfur reducing bacteria and methanogens within the ponds,
467 which degrade not only the residual bitumen (Holowenko et al., 2000; Percy, 2013; Quagraine et al.,
468 2005) but also the various components of naphtha (Shahimin and Siddique, 2017; Small et al., 2015).
469 Overall, tailings ponds emissions explain much of the TRS and CH_4 concentration variability in this data
470 set (Table 5) and in a recent aircraft study (Baray et al., 2018).

471 While component 1 correlates with CH_4 ($r = 0.59$), it does not correlate with CO_2 ($r = 0.09$). Emissions of
472 CH_4 from tailings ponds due to methanogenic bacterial activity are well-documented (Small et al., 2015;
473 Yeh et al., 2010) and hence the correlation with CH_4 is not unexpected. On the other hand, the lack of
474 correlation with CO_2 seems inconsistent with emission inventories that generally present tailings ponds
475 as large CO_2 sources (Small et al., 2015). One plausible explanation is that tailings ponds are a relatively

476 small CO₂ source overall in the region and that other, larger CO₂ sources and sinks (such as
477 photosynthesis and respiration by the vegetation surrounding the site) dominate the variance impacting
478 the PCA results. It may also indicate that, at least on aggregate and for the particular ponds detected in
479 this work, the emissions are in a regime where the release of CH₄ dominates over CO₂, i.e., the ponds
480 have, perhaps, become more anoxic than believed to be the case in previous studies and hence emit
481 more CH₄ (Holowenko et al., 2000). For example, Small et al. (2015) showed that older tailings ponds
482 (those without the addition of fresh froth or thickening treatments) tended to emit more CH₄, while
483 newer ponds are associated with higher VOC emissions. It is likely that component 1 is dominated by the
484 nearest pond (the Mildred Lake settling basin, 6 – 11 km SSE of AMS 13) and other tailings in the SE
485 where the majority of air samples originated from. The Mildred Lake settling basin is one of the oldest in
486 the region and is still actively being used; the correlation with CH₄ and VOC emissions is hence expected.

487 Component 1 is also associated with NO_y, rBC, CO, and HOA, though these correlations are relatively
488 modest ($r = 0.27, 0.30, 0.41, \text{ and } 0.40$, respectively). These species typically originate from combustion
489 sources, such as generators, motor vehicles, including diesel powered engines powering generators or
490 pumps; it is not obvious if and to what extent these are operated on or near tailings ponds, though.

491 Satellite observations have shown elevated concentrations of NO₂ above on-site upgrader facilities,
492 likely a result of emissions from extraction and transport sources (McLinden et al., 2012). In addition,
493 one of the major highways of the region is located adjacent to the Mildred Lake settling basin and other
494 major ponds in the region; highway traffic emissions (of CO, NO_y, rBC, and HOA) may hence also be
495 partially included in component 1.

496 The bivariate polar plot shows that component 1 was observed when local wind speeds were from the
497 SE and E of the measurement site (Fig. 5C), which is consistent with the notion that the Mildred Lake
498 settling basin and emissions along Highway 63 and, potentially, more distant facilities are sources
499 contributing to this component.

500 Component 1 is associated with the IVOC signature, though to a lesser degree than components 2 and 5.
501 The association of the IVOC signal with component 1 is slightly poorer ($r = 0.31$) than the association
502 with component 2 ($r = 0.39$), but significantly poorer than component 5 ($r = 0.74$). The association of
503 IVOCs with tailings ponds vapor can be explained by the presence of bitumen in the ponds that was not
504 separated from the sand during the separation stage (Holowenko et al., 2000). Tailings ponds contain
505 anywhere from 0.5% - 5% residual bitumen by weight (Chalaturnyk et al., 2002; Holowenko et al., 2000;
506 Penner and Foght, 2010). As illustrated in Fig. 4A, some of this material floats on the ponds' surfaces,
507 where IVOCs can partition to the air. Emission of IVOCs from bitumen floating on tailings ponds would
508 be a function of many variables (e.g., diluent composition, extraction methodology, settling rate,
509 temperature, etc.) and is thus not expected to be as persistent as CH_4 partitioning from the ponds to the
510 above air or from exposed bitumen on the mine surface, leading to a lower overall correlation.

511 Component 1 is also weakly associated with the less oxidized oxygenated organic aerosol factor, LO-
512 OOA ($r = 0.45$). Liggio et al. (2016) found that the observed secondary organic aerosol is dominated by
513 an OOA factor whose mass spectrum was similar to those of aerosols formed from oxidized bitumen
514 vapours. The organic aerosol budget in this study was also dominated by an OOA factor, the LO-OOA
515 (Lee et al., 2018). The association of LO-OOA with component 1 is thus consistent with its association
516 with IVOCs.

517 **4.1.2. Component 2: Mine fleet and vehicle emissions**

518 Component 2 strongly correlates with NO_y ($r = 0.82$), rBC ($r = 0.77$), pPAH ($r = 0.94$), and HOA ($r = 0.74$),
519 which suggests a combustion source such as diesel engines. In the AB oil sands, there is a sizeable off-
520 road mining truck fleet consisting of heavy aggregate haulers. In addition, there are diesel engine
521 sources associated with generators, pumps and land moving equipment, i.e., graders, dozers, hydraulic
522 excavators, and electric rope shovels (Watson et al., 2013; Wang et al., 2016). Most of these non-road

523 applications have been exempt from highway fuel taxes, on-road fuel formulation requirements and
524 after-engine exhaust treatment (Watson et al., 2013). Emissions from the hauler fleet and the stationary
525 sources would fit the profile of component 2. Other diesel engines operated in the region include a
526 commuter bus fleet, pickup and delivery trucks, tractor-trailers, and privately owned diesel powered
527 automobiles used to commute from the work sites to the major residential areas around Fort
528 McMurray, whose emissions are likely captured by component 2 as well, though the magnitude of these
529 relative to the mining truck fleet is not known. Consistent with component 2 being associated with an
530 anthropogenic source is its poor correlation with undecane ($r = 0.27$), likely arising from fugitive fuel
531 emissions.

532 The bivariate polar plot (Fig. 5D) for component 2 and NO_y in particular (Fig. S-4A) match the location of
533 Highway 63 which crosses the river to the SE of AMS 13 and bends to the E and is indicative of a line
534 source. At the same time, some of the largest mining operations in the region, the Susan Lake Gravel Pit,
535 Aurora North, Muskeg river, and Millennium mines are located to the NE and SE of AMS 13 as well. NO_y ,
536 rBC, and HOA (Fig. S-4A, B and D) all appear to have dominating point sources to the S and E when wind
537 speeds are $1\text{-}2 \text{ m s}^{-1}$. These directions are the same as the Fort McKay industrial park to the E and the
538 Syncrude Mildred Lake facility parking lot to the S which would have a higher concentration of vehicles
539 emitting these pollutants in a smaller area, whose emissions would be in addition to those from
540 industrial activities.

541 Component 2 is associated with the IVOCs signature and CH_4 (both $r = 0.39$). The mining activities bring
542 bitumen to the surface; similar to what we had observed in lab experiments (Fig. 2, black trace), the
543 surface exposure of bitumen during mining and on-site processing is expected to be associated with
544 fugitive emissions of CH_4 (Johnson et al., 2016) and IVOCs.

545 Fine-fraction particle-surface bound PAHs (pPAH) are associated strongly with component 2, but no

546 other components. Measurements of individual PAHs in snow and moss downwind from the oil sands
547 facilities have identified multiple sources of PAHs in the Athabasca oil sands, which include wind-blown
548 petroleum coke dust (also referred to as petcoke for short), a carbonaceous residual product from the
549 upgrading of crude petroleum that is stockpiled on mine sites, and emissions from fine tailings, oil sands
550 ore, and naturally exposed bitumen (Zhang et al., 2016; Jautzy et al., 2015; Parajulee and Wania, 2014).
551 Given this diversity of known sources, the associations of PAHs with only a single component is
552 surprising, though indicates that emissions from the mining fleet (which would include diesel and,
553 perhaps, wind-blown emissions from petcoke that is being transported) gave rise to most of the
554 variability in surface-bound PAH concentrations in this data set. The petcoke emissions identified in the
555 studies mentioned above are likely mainly associated with larger, supermicron sized particles, whose
556 PAH content would not be detected by the pPAH measurement in this data set.

557 Component 2 is not significantly associated with LO-OOA ($r = 0.11$), even though IVOCs are associated
558 with this component. This feature may indicate that the IVOCs emitted in component 2 are qualitatively
559 different from those emitted by components 1 and 5, in that they are less likely to yield organic aerosol
560 on the time scale of transport from emission to observation. One reason for the difference could be that
561 the bitumen that is transported by the mining fleet is relatively freshly exposed, whereas the IVOCs
562 released by bitumen in tailings ponds has been processed by microbes and that released by mine faces
563 (component 5) may have been photochemically oxidized to a greater extent and hence more prone to
564 rapid aerosol formation.

565 There is little to no association of component 2 with CO_2 ($r = 0.08$). This is somewhat unexpected as the
566 trucks are expected to release CO_2 (Wang et al., 2016) but could be due to significantly larger CO_2
567 sources in the area dominating the observed CO_2 variability at AMS 13 (e.g., components 3 and 6).
568 Furthermore, one would expect an association of non-road mining truck emissions with aromatics and
569 alkanes. Component 2 exhibited only poor correlations with decane ($r = 0.22$) and undecane ($r = 0.27$)

570 and negligible correlation with o-xylene ($r = 0.08$), suggesting that other components (i.e., component 1)
571 explained most of the variability of their concentrations at this site.

572

573 **4.1.3. Component 5: Surface-exposed bitumen and hot-water bitumen extraction**

574 Component 5 correlates more strongly with the IVOCs ($r = 0.74$) than with any other component and
575 correlates strongly with LO-OOA ($r = 0.72$), weakly with rBC ($r = 0.44$), and poorly with HOA ($r = 0.25$),
576 NO_y ($r = 0.22$), decane ($r = 0.23$), undecane ($r = 0.20$), and TRS ($r = 0.26$). We interpret this profile as
577 emissions from surface-exposed bitumen which outgases IVOCs.

578 One possibility is that these emissions occur on mine faces, where previously unexposed bitumen is
579 brought to the surface as a result of mining. Only a relatively small portion of the mine faces is actively
580 mined; those parts give rise to rBC and NO_y emissions from combustion engines in heavy haulers or
581 generators powering equipment. The poor association of component 5 with TRS could be due to sulfur
582 reducing bacteria found on the surface of bitumen. However, most of the variability of TRS at AMS 13 is
583 attributed to composite or “dry” tailings ponds given their more conducive environment to microbial
584 activity.

585 Component 5 does not correlate with CO_2 ($r = -0.03$) and only poorly with CH_4 ($r = 0.12$), which is
586 somewhat at odds with the notion of mine faces as the main source of IVOCs. The mine faces give rise to
587 substantial fugitive emissions of CO_2 and CH_4 (Johnson et al., 2016) – these emissions are likely captured
588 by component 6 in this analysis (see S.I.). It is unclear to what extent these greenhouse gases are
589 released relatively quickly from “hot spots” (i.e., from a small number of locations) through surface
590 cracks and fissures or by slow release from new material that is exposed and then releases greenhouse
591 gases during material handling, transport and processing (Johnson et al., 2016). IVOCs from surface-
592 exposed bitumen are likely released by the latter mechanism and are temperature-dependent. If the

593 mine faces are indeed the main IVOC source, the analysis results presented here suggest that the IVOCs
594 emissions from surface-exposed bitumen on mine faces are decoupled from CH₄ emissions in time and
595 appear as a distinct component and hence corroborate the "hot spots" or fast release hypothesis,
596 though clearly, more work is needed to characterize greenhouse gas emissions from oil sands mine
597 faces.

598 The association of IVOCs with component 5 may also be a result of fugitive emissions during the hot
599 water-based extraction of bitumen sand slurries during the separation phase of bitumen treatment.

600 Generally, bitumen is extracted in a weak alkaline environment by aeration of the solution to optimize
601 the separation of sand and bitumen (Masliyah et al., 2004). Unrecovered bitumen and naphtha then end
602 up in tailings. The recovered bitumen and naphtha are moved to upgrader facilities where they undergo
603 further treatment (such as coking or hydrotreatment). The magnitude of fugitive emissions during these
604 downstream extraction processes could be large, considering the bitumen is heated and actively
605 aerated. Future work should investigate IVOC fluxes near extraction plants and on mine faces.

606 Finally, it is conceivable that a "natural" background of IVOCs exists in the region (since bitumen can be
607 found at or near the surface in many parts of the region); such a natural background would also be
608 included in component 5. However, this "natural" bitumen would have been exposed at the surface for
609 geological time scales and, unlike unexposed, buried bitumen, likely would have lost most of its volatile
610 content over that period. Furthermore, the mine faces occupy large swaths of land in the region (as
611 evident from satellite imagery). Thus, the IVOCs emissions are more likely due to anthropogenic activity
612 than due to a natural phenomenon.

613

614 **4.2. Sources not associated with IVOCs**

615 **4.2.1. Component 3: Biogenic emissions and respiration**

616 Component 3 is strongly correlated with the monoterpenes α -pinene ($r = 0.98$), β -pinene ($r = 0.98$) and
617 limonene ($r = 0.92$) and is hence identified as a biogenic emissions source. This component is also weakly
618 associated with CO_2 ($r = 0.48$).

619 At AMS 13, CO_2 and the monoterpenes exhibit a very similar diurnal cycle: they are present in higher
620 concentrations during the night than during the day (Fig. 3) due to a decrease in the boundary layer
621 height (BLH) at night coupled with plant respiration of CO_2 and non-photochemical emission of
622 monoterpenes (Fares et al., 2013; Guenther et al., 2012). During the day, mixing ratios of CO_2 are lower
623 due to plant uptake and photosynthesis, and mixing ratios of terpenes are lower due to higher mixing
624 heights and vertical entrainment and due to oxidation by O_3 and OH (Fuentes et al., 1996). Hence, the
625 PCA gives a *positive* correlation of monoterpenes with CO_2 even though the physical processes,
626 photosynthesis and respiration, work in opposite direction.

627 The bivariate polar plots (Fig. S-5A-C) show that the monoterpenes and CO_2 were observed in highest
628 concentrations when the wind speeds were low ($< 1 \text{ m s}^{-1}$), consistent with formation of a stable
629 nocturnal boundary layer.

630 To corroborate this interpretation, the PCA was repeated with BLH estimated by a light detection and
631 ranging (LIDAR) instrument (Strawbridge et al., in prep.) added as a variable (Table S-9 in the S.I.). Since
632 BLH is not "emitted" by any source, it appears as a single variable component ($r = 0.90$). The only other
633 component that BLH (anti)correlates with is the biogenic component 3 ($r = -0.35$).

634 The dominant monoterpene species observed was α -pinene, followed by β -pinene and limonene,
635 though occasionally there was twice as much β -pinene than α -pinene in the sampled air. Some
636 variability of this ratio is expected since emission factors vary considerably between tree species (Geron
637 et al., 2000) which are not homogeneously distributed throughout the region (e.g., Fig. S1 of Rooney et
638 al. (2012)).

639 Simpson et al. (2010) observed enhancements of α -pinene and, to a greater extent, β -pinene over the
640 oil sands (up to 217 pptv and 610 pptv) compared to background levels of 20 ± 7 and 84 ± 24 pptv,
641 respectively, during mid-day overflights (which occurred between 11:00 and 13:00 local time). Similar
642 enhancements were also reported by Li et al. (2017) who observed emissions of biogenic hydrocarbons
643 in the four facilities sampled, three of which showed a higher β - than α -pinene concentration. The PCA
644 analysis (Table 5) showed no significant correlation of α - and β -pinene with any of the anthropogenic
645 sources, which implies that the biogenic source strength is simply too large for any anthropogenic
646 emissions of terpenes to be picked up in the analysis, especially considering that terpenes are relatively
647 short-lived.

648 The biogenic source shows poor anticorrelations with NO_y ($r = -0.26$), NH_3 ($r = -0.24$), and SO_2 ($r = -0.15$).
649 Many NO_y species (i.e., NO_2 , HONO, peroxy-carboxylic nitric anhydrides or PAN, and HNO_3) and SO_2
650 deposit to the forest canopy (Hsu et al., 2016; Min et al., 2014; Fenn et al., 2015); at night, when mixing
651 heights are lower, their concentrations are expected to decrease faster than during the day and are thus
652 out of phase with the CO_2 and terpene concentrations. In addition, there is a time-of-day observation
653 bias for SO_2 and, to lesser extent, NO_y , which are found in upgrader plumes (see 4.2.2.). The poor
654 anticorrelation with NH_3 likely arises because the NH_3 emissions from plants are mainly stomatal and
655 scale with temperature and are hence larger during the day than at night, anticorrelated with the
656 terpene source (Whaley et al., 2017).

657 **4.2.2 Component 4: Upgrader emissions**

658 Component 4 is strongly correlated with SO_2 ($r = 0.97$) and total sulfur ($r = 0.93$). By far the largest
659 source of SO_2 in the region are upgrader facilities, which emit as much as 6×10^7 kg annually according to
660 emission inventories (ECCC, 2013). Significant SO_2 emissions from upgrader facilities have recently been
661 confirmed by aircraft studies (Simpson et al., 2010; Howell et al., 2014; Liggio et al., 2016). Component 4

662 is also poorly correlated with NO_y ($r = 0.21$) but not with rBC ($r = 0.05$), consistent with a non-sooty (i.e.,
663 lean) combustion source such as upgrader stacks. Strong enhancements in SO_2 were only observed
664 intermittently as "spikes", which is expected when sampling emissions from relatively few and discrete
665 point sources.

666 Component 4 is poorly anticorrelated with CO_2 ($r = -0.12$), even though inventories indicate that the
667 upgrading facilities are the largest CO_2 source in the region (Furimsky, 2003; Englander et al., 2013; Yeh
668 et al., 2010). In this data set, the lack of correlation of component 4 with CO_2 (and to some extent with
669 PM_{10-1} as well) likely arises mainly from a sampling bias as stack emissions were only observed during
670 daytime, likely due to diurnal variability of the atmospheric boundary layer structure as explained
671 below.

672 Most of the variability in CO_2 concentration at AMS 13 is due to surface-based sources that originate
673 from large areas, especially biogenic processes (photosynthesis during the day and respiration at night,
674 component 3) and anthropogenic surface sources such as those captured by component 6 (section
675 4.2.3). Other anthropogenic pollutants, such as SO_2 , NO_y , and CH_4 , are not subject to large biogenically
676 driven processes and are less affected than CO_2 .

677 In contrast to surface sources, emissions from the > 100 m tall stacks are comparatively undersampled
678 and observed mainly during daytime, when vertical mixing brings elevated plumes to the surface, yet
679 CO_2 concentrations are generally much lower than during the night due to uptake by vegetation. At
680 night, pollutants emitted from stacks are injected above the likely very shallow nocturnal surface layer
681 and were hence not observed at the surface. Vertical profile measurements of SO_2 stack plumes by a
682 Pandora spectral sun photometer at Fort McKay during daytime have shown considerable vertical
683 gradients and only occasional transport of SO_2 all the way to the surface (Fioletov et al., 2016).

684 The association of component 4 with CO_2 is negative because the stack emission source is observed only

685 during the day when the large biogenic sink dominates and effectively masks the relatively small
686 increase due to anthropogenic CO₂. In contrast, background concentrations of SO₂ are comparatively
687 low, and the increase in SO₂ concentrations is readily picked up the PCA.

688 It would be interesting to conduct a future study in winter when biogenic activities decrease; a
689 wintertime PCA analysis of surface measurements might be able to associate CO₂ enhancements with
690 upgraders, though boundary layer mixing heights would decrease as well, which would make a PCA
691 analysis using surface data even more challenging.

692 Component 4 does not correlate with PM₁₀₋₁ volume ($r = 0.09$). It is clear that the emitted SO₂ will
693 contribute to secondary aerosol formation downwind, such that a correlation of stack emissions with
694 PM₁₀₋₁ volume might be expected. However, these secondary contributions will likely mostly be in the
695 submicron aerosol fraction, which adds relatively little to PM₁₀₋₁ volume. Further, PM₁₀₋₁ volume is
696 dominated by coarse particles from other primary sources, mostly wind-blown emission of sand from
697 the mine surfaces, roadways and, perhaps, bioaerosol (component 7, see S.I.). These effects make PM₁₀₋₁
698 volume from stacks appear comparatively small, such that the variability of the larger, surface-based
699 sources likely masks the contribution of stacks emissions to PM₁₀₋₁ variability.

700 The bivariate polar plot of component 4 (Fig. S-6D) shows that the largest magnitudes were observed
701 when local winds were from the SE. The corresponding plot of SO₂ (Fig. S-6A) reveals two more distinct
702 sources: a larger one from the E and a smaller one from the SSE. However, only two facilities (Sunrise
703 and Firebag) are located to the E at relatively large distances of 37 km and 47 km respectively. The
704 largest known upgraders and SO₂ sources in the area (i.e., upgraders located at the Mildred Lake and
705 Suncor base plants) are located to the S and SE of AMS 13. Considering that the stack emissions are only
706 observed intermittently, we speculate that there exists a mesoscale transport pattern in the Athabasca
707 river valley which channel emissions, such that the local wind direction and speed may be misleading as

708 to the true location of these sources. For more extensive data sets, such phenomena may very well
709 average out but perhaps did not in this case.

710 **4.3. Extended PCA with added secondary variables**

711 The extended analysis (Table 7) qualitatively preserves the structure (with the exception of an added
712 “Aged” component, # 6) of the original 10-component solution but allows an assessment of which
713 components most result in formation of secondary products such as SOA, which has implications for
714 health (Bernstein, 2004) and climate (Charlson et al., 1992). Secondary products vary considerably as a
715 function of air mass chemical age (which depends, amongst other components, on time of day and
716 synoptic conditions, including wind speed) and are hence expected to add considerable noise and
717 scatter to the results leading to lower correlations. On the other hand, the distance between the
718 measurement site and sources is fixed, such that this variability should average out over time. This
719 indeed appears to have happened in this data set in spite of the relatively low sample size.

720 The analysis indicates that the component with the strongest IVOC source (Component 5) also has the
721 highest association with PM_1 ($r = 0.7$; Table 7). Aircraft measurements combined with a modelling study
722 have required a group of IVOC hydrocarbons to explain the significant SOA formation and growth
723 downwind of the oil sands region (Liggio et al., 2016). The association of IVOCs with PM_1 volume is
724 consistent with the hypothesis that oxidation of IVOCs observed at AMS 13 leads to SOA generation and
725 appears to have a significant impact on the variation in PM_1 mass.

726 The second component influencing PM_1 is that from stack emissions (Component 4 in the primary PCA;
727 Component 2 in the secondary PCA) (Tables 5 and 7). It is well established that the oxidation of SO_2 to
728 sulfate will lead to formation of fine particulate matter. This apparently occurs, at least partially, on the
729 time scale between the point of emission and the AMS 13 site (assuming a wind speed of 3 m/s and a
730 distance of 11 km, the transit time is 1 hour), though some fraction of $SO_4^{2-}(p)$ is likely directly emitted.

731

732 **5. Summary and conclusions**

733 A PCA was applied to continuous measurements of 22 primary pollutant tracers at the AMS 13 ground
734 site in the Athabasca oil sands during the 2013 JOSM intensive study to elucidate the origins of airborne
735 analytically unresolved hydrocarbons that were observed by GC-ITMS. The analysis identified 10
736 components. Three components correlated with the IVOC signature and were assigned to mine faces
737 and, potentially, hot-water bitumen extraction facilities, the mine hauler fleet, and wet tailings ponds
738 emissions. All three are anthropogenic activities that involve the handling of raw bitumen, i.e., the
739 unearthing, mining and transport of crude bitumen, and the disposal of processed material that contains
740 residual bitumen in wet tailings ponds. The PCA results are consistent with our previous interpretation
741 that the unresolved hydrocarbons originate from bitumen, which was based on the similarity of the
742 chromatograms with those obtained in a head space vapor analysis of ground-up bitumen in the
743 laboratory.

744 Liggio et al. (2016) showed that these hydrocarbons constitute a group of IVOCs in the saturation vapor
745 concentration (C^*) range $10^5 \mu\text{g m}^{-3} < C^* < 10^7 \mu\text{g m}^{-3}$ that contribute significantly to secondary organic
746 aerosol formation and growth downwind of the oil sands facilities. The correlation of LO-OOA with two
747 of the three IVOC components in the main PCA analysis and with PM_{10} in the extended analysis
748 corroborates the high SOA formation potential of IVOCs and suggests that further differentiation may be
749 needed and stresses the need for IVOCs to be routinely monitored. In particular, direct measurements
750 of emissions throughout the processing of raw bitumen are needed to pinpoint source contributions
751 more accurately and aid in the development of potential mitigation strategies.

752 The PCA analysis in this study suffered from several limitations. For instance, PCA does not provide
753 insight into emission factors of individual facilities, though it does capture what conditions change

754 ambient concentrations the most. Further, the receptor nature of PCA did not always discern between
755 large source areas that may have many individual point sources coming together at the point of
756 observation. For example, component 1 contains an obvious tailings pond signature because of its high
757 correlations with anthropogenic VOCs, methane and TRS, but also includes several combustion sources,
758 making interpretation of this IVOC source location more challenging. A longer continuous data set with a
759 greater number of variables would have perhaps been able to resolve these different sources, including
760 the various tailings ponds, of which there are 19 in the region, all with slightly different emission profiles
761 (Small et al., 2015) .

762 Another limitation is the bias of this (and most) ground site data set towards surface-based emissions
763 and the undersampling of stack emissions. Facility stacks were only observed in the daytime because at
764 night the mixing height is so low that the stacks are emitting directly into the residual layer. These
765 emissions could be quantified using aircraft based platforms (Howell et al., 2014; Li et al., 2017; Baray et
766 al., 2018). The PCA struggled most with the allocation of greenhouse gases. Mixing ratios of CO₂, in
767 particular, were difficult to reconcile in this analysis due to a high background and large attenuation by
768 biogenic activity and boundary layer meteorology. Forests greatly affected CO₂ levels in the region
769 because it is taken up during the day when plants are photosynthetically active and emitted at night
770 when plants undergo cellular respiration. This CO₂ source and sink appears to dominate the PCA,
771 effectively masking relatively small emissions from tailings ponds, facilities, and tail pipes in particular
772 from the mine hauling fleet.

773 Finally, there is a need for improved monitoring methods for IVOCs. For instance, future studies should
774 focus on characterizing the VOCs in the above mentioned volatility range using a greater mass and time
775 resolution instrument, such as a time-of-flight mass spectrometer (TOF-MS) or higher resolution
776 separation methods (e.g., multi-dimensional gas chromatography), and also include measurement of
777 speciated aerosol organic composition by, for example, thermal desorption aerosol GC (TAG) analysis

778 (Williams et al., 2006). Future studies should also investigate how IVOC volatility distributions vary with
779 source type and chemical age.

780 **Acknowledgments**

781 Funding for this study was provided by Environment and Climate Change Canada and the Canada-
782 Alberta Oil Sands Monitoring program. The GC-ITMS used in this work was purchased using funds
783 provided by the Canada Foundation for Innovation and matching funds by the Alberta government.
784 TWT, JAH, DKB, FVA and GRW acknowledge financial support from the Natural Sciences and Engineering
785 Research Council of Canada (NSERC) Collaborative Research and Training Experience Program (CREATE)
786 program Integrating Atmospheric Chemistry and Physics from Earth to Space (IACPES).

787 **6. References**

- 788 Government of Alberta, oil sands information portal: <http://osip.alberta.ca>, access: 23-FEB-2017, 2017.
- 789 Allen, E. W.: Process water treatment in Canada's oil sands industry: II. A review of emerging
790 technologies, *J. Environ. Eng. Sci.*, 7, 499-524, 10.1139/s08-020, 2008.
- 791 Baray, S., Darlington, A., Gordon, M., Hayden, K. L., Leithead, A., Li, S. M., Liu, P. S. K., Mittermeier, R. L.,
792 Moussa, S. G., O'Brien, J., Staebler, R., Wolde, M., Worthy, D., and McLaren, R.: Quantification of
793 methane sources in the Athabasca Oil Sands Region of Alberta by aircraft mass balance, *Atmos.*
794 *Chem. Phys.*, 18, 7361-7378, 10.5194/acp-18-7361-2018, 2018.
- 795 Bari, M., and Kindzierski, W. B.: Fifteen-year trends in criteria air pollutants in oil sands communities of
796 Alberta, Canada, *Environ. Int.*, 74, 200-208, 10.1016/j.envint.2014.10.009, 2015.
- 797 Bernstein, D. M.: Increased mortality in COPD among construction workers exposed to inorganic dust,
798 *Eur. Resp. J.*, 24, 512-512, 10.1183/09031936.04.00044504, 2004.
- 799 Bond, T. C., Streets, D. G., Yarber, K. F., Nelson, S. M., Woo, J. H., and Klimont, Z.: A technology-based
800 global inventory of black and organic carbon emissions from combustion, *J. Geophys. Res.*, 109,
801 D14203, 10.1029/2003JD003697, 2004.
- 802 Briggs, N. L., and Long, C. M.: Critical review of black carbon and elemental carbon source
803 apportionment in Europe and the United States, *Atmos. Environ.*, 144, 409-427,
804 10.1016/j.atmosenv.2016.09.002, 2016.
- 805 Buhamra, S. S., Bouhamra, W. S., and Elkilani, A. S.: Assessment of air quality in ninety-nine residences of
806 Kuwait, *Environ. Technol.*, 19, 357-367, 10.1080/09593331908616691, 1998.
- 807 Burtscher, H., Scherrer, L., Siegmann, H. C., Schmidtott, A., and Federer, B.: Probing aerosols by
808 photoelectric charging, *J. Appl. Phys.*, 53, 3787-3791, 10.1063/1.331120, 1982.
- 809 Bytnerowicz, A., Fraczek, W., Schilling, S., and Alexander, D.: Spatial and temporal distribution of
810 ambient nitric acid and ammonia in the Athabasca Oil Sands Region, Alberta, *J. Limnol.*, 69, 11-21,
811 10.3274/jl10-69-s1-03, 2010.
- 812 The facts on Canada's oil sands: <http://www.capp.ca/publications-and-statistics/publications/296225>,
813 access: April 20, 2017, 2016.
- 814 Carslaw, D. C., and Ropkins, K.: openair - An R package for air quality data analysis, *Environ. Modell.*
815 *Softw.*, 27-28, 52-61, 10.1016/j.envsoft.2011.09.008, 2012.
- 816 Carslaw, D. C., and Beevers, S. D.: Characterising and understanding emission sources using bivariate
817 polar plots and k-means clustering, *Environ. Modell. Softw.*, 40, 325-329,
818 10.1016/j.envsoft.2012.09.005, 2013.
- 819 Cattell, R. B.: The Scree Test For The Number Of Factors, *Multivariate Behavioral Research*, 1, 245-276,
820 10.1207/s15327906mbr0102_10, 1966.
- 821 Chalaturnyk, R. J., Don Scott, J., and Ozum, B.: Management of oil sands tailings, *Petroleum Science and*
822 *Technology*, 20, 1025-1046, 10.1081/lft-120003695, 2002.
- 823 Charlson, R. J., Schwartz, S. E., Hales, J. M., Cess, R. D., Coakley, J. A., Hansen, J. E., and Hofmann, D. J.:
824 Climate forcing by anthropogenic aerosols, *Science*, 255, 423-430, 10.1126/science.255.5043.423
825 1992.
- 826 Chen, H., Karion, A., Rella, C. W., Winderlich, J., Gerbig, C., Filges, A., Newberger, T., Sweeney, C., and
827 Tans, P. P.: Accurate measurements of carbon monoxide in humid air using the cavity ring-down
828 spectroscopy (CRDS) technique, *Atmos. Meas. Tech.*, 6, 1031-1040, 10.5194/amt-6-1031-2013, 2013.
- 829 Cross, E. S., Hunter, J. F., Carrasquillo, A. J., Franklin, J. P., Herndon, S. C., Jayne, J. T., Worsnop, D. R.,
830 Miake-Lye, R. C., and Kroll, J. H.: Online measurements of the emissions of intermediate-volatility and
831 semi-volatile organic compounds from aircraft, *Atmos. Chem. Phys.*, 13, 7845-7858, 10.5194/acp-13-
832 7845-2013, 2013.

833 de Gouw, J. A., Middlebrook, A. M., Warneke, C., Ahmadov, R., Atlas, E. L., Bahreini, R., Blake, D. R.,
834 Brock, C. A., Brioude, J., Fahey, D. W., Fehsenfeld, F. C., Holloway, J. S., Le Henaff, M., Lueb, R. A.,
835 McKeen, S. A., Meagher, J. F., Murphy, D. M., Paris, C., Parrish, D. D., Perring, A. E., Pollack, I. B.,
836 Ravishankara, A. R., Robinson, A. L., Ryerson, T. B., Schwarz, J. P., Spackman, J. R., Srinivasan, A., and
837 Watts, L. A.: Organic Aerosol Formation Downwind from the Deepwater Horizon Oil Spill, *Science*,
838 331, 1295-1299, 10.1126/science.1200320, 2011.

839 Trends in atmospheric methane: www.esrl.noaa.gov/gmd/ccgg/trends_ch4/, access: April 11, 2017,
840 2017a.

841 Trends in atmospheric carbon dioxide: www.esrl.noaa.gov/gmd/ccgg/trends/, access: April 11, 2017,
842 2017b.

843 National pollutant release inventory (NPRI): [http://open.canada.ca/data/en/dataset/e40099ae-b116-](http://open.canada.ca/data/en/dataset/e40099ae-b116-4c48-9475-f3806fe5a6a6)
844 [4c48-9475-f3806fe5a6a6](http://open.canada.ca/data/en/dataset/e40099ae-b116-4c48-9475-f3806fe5a6a6), access: October 5, 2016, 2013.

845 ECCC: Joint oil sands monitoring program emissions inventory compilation report, Environment and
846 Climate Change Canada, Downsview, 2016.

847 Englander, J. G., Bharadwaj, S., and Brandt, A. R.: Historical trends in greenhouse gas emissions of the
848 Alberta oil sands (1970-2010), *Environm. Res. Lett.*, 8, 044036, 10.1088/1748-9326/8/4/044036,
849 2013.

850 Fares, S., Schnitzhofer, R., Jiang, X., Guenther, A., Hansel, A., and Loreto, F.: Observations of Diurnal to
851 Weekly Variations of Monoterpene-Dominated Fluxes of Volatile Organic Compounds from
852 Mediterranean Forests: Implications for Regional Modeling, *Environm. Sci. Technol.*, 47, 11073-
853 11082, 10.1021/es4022156, 2013.

854 Fenn, M. E., Bytnerowicz, A., Schilling, S. L., and Ross, C. S.: Atmospheric deposition of nitrogen, sulfur
855 and base cations in jack pine stands in the Athabasca Oil Sands Region, Alberta, Canada, *Environ.*
856 *Pollut.*, 196, 497-510, 10.1016/j.envpol.2014.08.023, 2015.

857 Fioletov, V. E., McLinden, C. A., Cede, A., Davies, J., Mihele, C., Netcheva, S., Li, S. M., and O'Brien, J.:
858 Sulfur dioxide (SO₂) vertical column density measurements by Pandora spectrometer over the
859 Canadian oil sands, *Atmospheric Measurement Techniques*, 9, 2961-2976, 10.5194/amt-9-2961-
860 2016, 2016.

861 Fuentes, J. D., Wang, D., Neumann, H. H., Gillespie, T. J., DenHartog, G., and Dann, T. F.: Ambient
862 biogenic hydrocarbons and isoprene emissions from a mixed deciduous forest, *J. Atmos. Chem.*, 25,
863 67-95, 10.1007/BF00053286, 1996.

864 Furimsky, E.: Emissions of carbon dioxide from tar sands plants in Canada, *Energy Fuels*, 17, 1541-1548,
865 10.1021/ef0301102, 2003.

866 Geron, C., Rasmussen, R., Arnts, R. R., and Guenther, A.: A review and synthesis of monoterpene
867 speciation from forests in the United States, *Atmos. Environm.*, 34, 1761-1781, 10.1016/S1352-
868 2310(99)00364-7, 2000.

869 Gordon, M., Li, S. M., Staebler, R., Darlington, A., Hayden, K., O'Brien, J., and Wolde, M.: Determining air
870 pollutant emission rates based on mass balance using airborne measurement data over the Alberta
871 oil sands operations, *Atmos. Meas. Tech.*, 8, 3745-3765, 10.5194/amt-8-3745-2015, 2015.

872 Grimmer, G., Brune, H., Deutschwenzel, R., Dettbarn, G., Jacob, J., Naujack, K. W., Mohr, U., and Ernst,
873 H.: Contribution of polycyclic aromatic-hydrocarbons and nitro-derivatives to the carcinogenic impact
874 of diesel-engine exhaust condensate evaluated by implantation into the lungs of rats, *Cancer Lett.*,
875 37, 173-180, 10.1016/0304-3835(87)90160-1, 1987.

876 Guenther, A. B., Jiang, X., Heald, C. L., Sakulyanontvittaya, T., Duhl, T., Emmons, L. K., and Wang, X.: The
877 Model of Emissions of Gases and Aerosols from Nature version 2.1 (MEGAN2.1): an extended and
878 updated framework for modeling biogenic emissions, *Geosci. Model Dev.*, 5, 1471-1492,
879 10.5194/gmd-5-1471-2012, 2012.

880 Guo, H., Wang, T., and Louie, P. K. K.: Source apportionment of ambient non-methane hydrocarbons in
881 Hong Kong: Application of a principal component analysis/absolute principal component scores
882 (PCA/APCS) receptor model, *Environ. Pollut.*, 129, 489-498, 10.1016/j.envpol.2003.11.006, 2004.

883 Hair, J. F., Anderson, R. E., Tatham, R. L., and Black, W. C.: *Multivariate data analysis*, in, 7th edition ed.,
884 Prentice-Hall, Upper Saddle River, NJ, pp. 108 -110, 1998.

885 Harrison, R. M., Smith, D. J. T., and Luhana, L.: Source apportionment of atmospheric polycyclic aromatic
886 hydrocarbons collected from an urban location in Birmingham, UK, *Environ. Sci. Technol.*, 30, 825-
887 832, 10.1021/es950252d, 1996.

888 Helmig, D., Klinger, L. F., Guenther, A., Vierling, L., Geron, C., and Zimmerman, P.: Biogenic volatile
889 organic compound emissions (BVOCs) I. Identifications from three continental sites in the U.S,
890 *Chemosphere*, 38, 2163-2187, 10.1016/S0045-6535(98)00425-1, 1999.

891 Holowenko, F. M., MacKinnon, M. D., and Fedorak, P. M.: Methanogens and sulfate-reducing bacteria in
892 oil sands fine tailings waste, *Canadian Journal of Microbiology*, 46, 927-937, 10.1139/cjm-46-10-927,
893 2000.

894 Howell, S. G., Clarke, A. D., Freitag, S., McNaughton, C. S., Kapustin, V., Brekovskikh, V., Jimenez, J. L.,
895 and Cubison, M. J.: An airborne assessment of atmospheric particulate emissions from the processing
896 of Athabasca oil sands, *Atmos. Chem. Phys.*, 14, 5073-5087, 10.5194/acp-14-5073-2014, 2014.

897 Hsu, Y. M., Bytnerowicz, A., Fenn, M. E., and Percy, K. E.: Atmospheric dry deposition of sulfur and
898 nitrogen in the Athabasca Oil Sands Region, Alberta, Canada, *Sci. Tot. Environm.*, 568, 285-295,
899 10.1016/j.scitotenv.2016.05.205, 2016.

900 Jautzy, J. J., Ahad, J. M. E., Gobeil, C., Smirnoff, A., Barst, B. D., and Savard, M. M.: Isotopic Evidence for
901 Oil Sands Petroleum Coke in the Peace-Athabasca Delta, *Environm. Sci. Technol.*, 49, 12062-12070,
902 10.1021/acs.est.5b03232, 2015.

903 Jimenez, J. L., Canagaratna, M. R., Donahue, N. M., Prevot, A. S. H., Zhang, Q., Kroll, J. H., DeCarlo, P. F.,
904 Allan, J. D., Coe, H., Ng, N. L., Aiken, A. C., Docherty, K. S., Ulbrich, I. M., Grieshop, A. P., Robinson, A.
905 L., Duplissy, J., Smith, J. D., Wilson, K. R., Lanz, V. A., Hueglin, C., Sun, Y. L., Tian, J., Laaksonen, A.,
906 Raatikainen, T., Rautiainen, J., Vaattovaara, P., Ehn, M., Kulmala, M., Tomlinson, J. M., Collins, D. R.,
907 Cubison, M. J., E., Dunlea, J., Huffman, J. A., Onasch, T. B., Alfarra, M. R., Williams, P. I., Bower, K.,
908 Kondo, Y., Schneider, J., Drewnick, F., Borrmann, S., Weimer, S., Demerjian, K., Salcedo, D., Cottrell,
909 L., Griffin, R., Takami, A., Miyoshi, T., Hatakeyama, S., Shimono, A., Sun, J. Y., Zhang, Y. M., Dzepina,
910 K., Kimmel, J. R., Sueper, D., Jayne, J. T., Herndon, S. C., Trimborn, A. M., Williams, L. R., Wood, E. C.,
911 Middlebrook, A. M., Kolb, C. E., Baltensperger, U., and Worsnop, D. R.: Evolution of Organic Aerosols
912 in the Atmosphere, *Science*, 326, 1525-1529, 10.1126/science.1180353, 2009.

913 Johnson, M. R., Crosland, B. M., McEwen, J. D., Hager, D. B., Armitage, J. R., Karimi-Golpayegani, M., and
914 Picard, D. J.: Estimating fugitive methane emissions from oil sands mining using extractive core
915 samples, *Atmos. Environm.*, 144, 111-123, 10.1016/j.atmosenv.2016.08.073, 2016.

916 Jolliffe, I. T., and Cadima, J.: Principal component analysis: a review and recent developments,
917 *Philosophical Transactions of the Royal Society A: Mathematical, Physical and Engineering Sciences*,
918 374, 10.1098/rsta.2015.0202, 2016.

919 Kaiser, H. F.: The varimax criterion for analytic rotation in factor-analysis, *Psychometrika*, 23, 187-200,
920 10.1007/bf02289233, 1958.

921 Kindzierski, W. B., and Ranganathan, H. K. S.: Indoor and outdoor SO₂ in a community near oil sand
922 extraction and production facilities in northern Alberta, *J. Environ. Eng. Sci.*, 5, S121-S129,
923 10.1139/s06-022, 2006.

924 Lee, A. K. Y., Adam, M. G., Liggio, J., Li, S.-M., Li, K., Willis, M. D., Abbatt, J. P. D., Tokarek, T. W., Odame-
925 Ankrah, C. A., Huo, J. A., Osthoff, H. D., Strawbridge, K. B., and Brook, J. R.: A large contribution of
926 anthropogenic organonitrate to secondary organic aerosol in Alberta oil sands, in prep., 2018.

927 Li, S.-M., Leithead, A., Moussa, S. G., Liggio, J., Moran, M. D., Wang, D., Hayden, K., Darlington, A.,
928 Gordon, M., Staebler, R., Makar, P. A., Stroud, C. A., McLaren, R., Liu, P. S. K., O'Brien, J.,
929 Mittermeier, R. L., Zhang, J., Marson, G., Cober, S. G., Wolde, M., and Wentzell, J. J. B.: Differences
930 between measured and reported volatile organic compound emissions from oil sands facilities in
931 Alberta, Canada, *Proceedings of the National Academy of Sciences*, 114, E3756-E3765,
932 10.1073/pnas.1617862114, 2017.

933 Liggio, J., Li, S.-M., Hayden, K., Taha, Y. M., Stroud, C., Darlington, A., Drollette, B. D., Gordon, M., Lee, P.,
934 Liu, P., Leithead, A., Moussa, S. G., Wang, D., O'Brien, J., Mittermeier, R. L., Brook, J., Lu, G., Staebler,
935 R., Han, Y., Tokarek, T. W., Osthoff, H. D., Makar, P. A., Zhang, J., Plata, D., and Gentner, D. R.: Oil
936 Sands Operations as a Large Source of Secondary Organic Aerosols, *Nature*, 534, 91-94,
937 10.1038/nature17646, 2016.

938 Marey, H. S., Hashisho, Z., Fu, L., and Gille, J.: Spatial and temporal variation in CO over Alberta using
939 measurements from satellites, aircraft, and ground stations, *Atmos. Chem. Phys.*, 15, 3893-3908,
940 10.5194/acp-15-3893-2015, 2015.

941 Markovic, M. Z., VandenBoer, T. C., and Murphy, J. G.: Characterization and optimization of an online
942 system for the simultaneous measurement of atmospheric water-soluble constituents in the gas and
943 particle phases, *J. Environ. Monit.*, 14, 1872-1884, 10.1039/C2EM00004K, 2012.

944 Masliyah, J., Zhou, Z. J., Xu, Z. H., Czarnecki, J., and Hamza, H.: Understanding water-based bitumen
945 extraction from athabasca oil sands, *Can. J. Chem. Eng.*, 82, 628-654, 10.1002/cjce.5450820403,
946 2004.

947 McLinden, C. A., Fioletov, V., Boersma, K. F., Krotkov, N., Sioris, C. E., Veefkind, J. P., and Yang, K.: Air
948 quality over the Canadian oil sands: A first assessment using satellite observations, *Geophys. Res.
949 Lett.*, 39, 8, 10.1029/2011gl050273, 2012.

950 Miller, S. M., Matross, D. M., Andrews, A. E., Millet, D. B., Longo, M., Gottlieb, E. W., Hirsch, A. I., Gerbig,
951 C., Lin, J. C., Daube, B. C., Hudman, R. C., Dias, P. L. S., Chow, V. Y., and Wofsy, S. C.: Sources of carbon
952 monoxide and formaldehyde in North America determined from high-resolution atmospheric data,
953 *Atmos. Chem. Phys.*, 8, 7673-7696, 10.5194/acp-8-7673-2008, 2008.

954 Min, K. E., Pusede, S. E., Browne, E. C., LaFranchi, B. W., and Cohen, R. C.: Eddy covariance fluxes and
955 vertical concentration gradient measurements of NO and NO₂ over a ponderosa pine ecosystem:
956 observational evidence for within-canopy chemical removal of NO_x, *Atmos. Chem. Phys.*, 14, 5495-
957 5512, 10.5194/acp-14-5495-2014, 2014.

958 Nara, H., Tanimoto, H., Tohjima, Y., Mukai, H., Nojiri, Y., Katsumata, K., and Rella, C. W.: Effect of air
959 composition (N₂, O₂, Ar, and H₂O) on CO₂ and CH₄ measurement by wavelength-scanned cavity ring-
960 down spectroscopy: calibration and measurement strategy, *Atmos. Meas. Tech.*, 5, 2689-2701,
961 10.5194/amt-5-2689-2012, 2012.

962 Nimana, B., Canter, C., and Kumar, A.: Energy consumption and greenhouse gas emissions in the
963 recovery and extraction of crude bitumen from Canada's oil sands, *Appl. Energy*, 143, 189-199,
964 10.1016/j.apenergy.2015.01.024, 2015a.

965 Nimana, B., Canter, C., and Kumar, A.: Energy consumption and greenhouse gas emissions in upgrading
966 and refining of Canada's oil sands products, *Energy*, 83, 65-79, 10.1016/j.energy.2015.01.085, 2015b.

967 Detailed facility information: [http://www.ec.gc.ca/inrp-npri/donnees-](http://www.ec.gc.ca/inrp-npri/donnees-data/index.cfm?do=facility_information&lang=En&opt_npri_id=0000002274&opt_report_year=2013)
968 [data/index.cfm?do=facility_information&lang=En&opt_npri_id=0000002274&opt_report_year=2013](http://www.ec.gc.ca/inrp-npri/donnees-data/index.cfm?do=facility_information&lang=En&opt_npri_id=0000002274&opt_report_year=2013)
969 , access: April 13, 2017, 2013.

970 Odame-Ankrah, C. A.: Improved detection instrument for nitrogen oxide species, Ph.D., Chemistry,
971 University of Calgary, <http://hdl.handle.net/11023/2006>, Calgary, 2015.

972 Onasch, T. B., Trimborn, A., Fortner, E. C., Jayne, J. T., Kok, G. L., Williams, L. R., Davidovits, P., and
973 Worsnop, D. R.: Soot Particle Aerosol Mass Spectrometer: Development, Validation, and Initial
974 Application, *Aerosol Sci. Technol.*, 46, 804-817, 10.1080/02786826.2012.663948, 2012.

975 Paatero, P., and Tapper, U.: Positive matrix factorization: A non-negative factor model with optimal
976 utilization of error estimates of data values, *Environmetrics*, 5, 111-126,
977 doi:10.1002/env.3170050203, 1994.

978 Parajulee, A., and Wania, F.: Evaluating officially reported polycyclic aromatic hydrocarbon emissions in
979 the Athabasca oil sands region with a multimedia fate model, *Proceedings of the National Academy
980 of Sciences*, 111, 3344-3349, 10.1073/pnas.1319780111, 2014.

981 Paul, D., and Osthoff, H. D.: Absolute Measurements of Total Peroxy Nitrate Mixing Ratios by Thermal
982 Dissociation Blue Diode Laser Cavity Ring-Down Spectroscopy, *Anal. Chem.*, 82, 6695-6703,
983 10.1021/ac101441z, 2010.

984 Penner, T. J., and Foght, J. M.: Mature fine tailings from oil sands processing harbour diverse
985 methanogenic communities, *Canadian Journal of Microbiology*, 56, 459-470, 10.1139/w10-029, 2010.

986 Percy, K. E.: Ambient Air Quality and Linkage to Ecosystems in the Athabasca Oil Sands, Alberta, *Geosci.
987 Can.*, 40, 182-201, 10.12789/geocanj.2013.40.014, 2013.

988 Peters, T. M., and Leith, D.: Concentration measurement and counting efficiency of the aerodynamic
989 particle sizer 3321, *J. Aerosol Sci.*, 34, 627-634, 10.1016/s0021-8502(03)00030-2, 2003.

990 Quagraine, E. K., Headley, J. V., and Peterson, H. G.: Is biodegradation of bitumen a source of recalcitrant
991 naphthenic acid mixtures in oil sands tailing pond waters?, *J. Environ. Sci. Health Part A-Toxic/Hazard.
992 Subst. Environ. Eng.*, 40, 671-684, 10.1081/ese-200046637, 2005.

993 Rooney, R. C., Bayley, S. E., and Schindler, D. W.: Oil sands mining and reclamation cause massive loss of
994 peatland and stored carbon, *Proc. Natl. Acad. Sci. U.S.A.*, 109, 4933-4937, 10.1073/pnas.1117693108,
995 2012.

996 RStudio Boston, M.: Integrated development environment for R, 2017.

997 Shahimin, M. F. M., and Siddique, T.: Sequential biodegradation of complex naphtha hydrocarbons
998 under methanogenic conditions in two different oil sands tailings, *Environ. Pollut.*, 221, 398-406,
999 10.1016/j.envpol.2016.12.002, 2017.

1000 Siddique, T., Fedorak, P. M., and Foght, J. M.: Biodegradation of short-chain n-alkanes in oil sands
1001 tailings under methanogenic conditions, *Environ. Sci. Technol.*, 40, 5459-5464, 10.1021/es060993m,
1002 2006.

1003 Siddique, T., Gupta, R., Fedorak, P. M., MacKinnon, M. D., and Foght, J. M.: A first approximation kinetic
1004 model to predict methane generation from an oil sands tailings settling basin, *Chemosphere*, 72,
1005 1573-1580, 10.1016/j.chemosphere.2008.04.036, 2008.

1006 Siddique, T., Penner, T., Semple, K., and Foght, J. M.: Anaerobic Biodegradation of Longer-Chain n-
1007 Alkanes Coupled to Methane Production in Oil Sands Tailings, *Environm. Sci. Technol.*, 45, 5892-5899,
1008 10.1021/es200649t, 2011.

1009 Siddique, T., Penner, T., Klassen, J., Nesbo, C., and Foght, J. M.: Microbial Communities Involved in
1010 Methane Production from Hydrocarbons in Oil Sands Tailings, *Environ. Sci. Technol.*, 46, 9802-9810,
1011 10.1021/e53022024, 2012.

1012 Simpson, I. J., Blake, N. J., Barletta, B., Diskin, G. S., Fuelberg, H. E., Gorham, K., Huey, L. G., Meinardi, S.,
1013 Rowland, F. S., Vay, S. A., Weinheimer, A. J., Yang, M., and Blake, D. R.: Characterization of trace
1014 gases measured over Alberta oil sands mining operations: 76 speciated C₂-C₁₀ volatile organic
1015 compounds (VOCs), CO₂, CH₄, CO, NO, NO₂, NO_y, O₃ and SO₂, *Atmos. Chem. Phys.*, 10, 11931-11954,
1016 10.5194/acp-10-11931-2010, 2010.

1017 Small, C. C., Cho, S., Hashisho, Z., and Ulrich, A. C.: Emissions from oil sands tailings ponds: Review of
1018 tailings pond parameters and emission estimates, *Journal of Petroleum Science and Engineering*, 127,
1019 490-501, 10.1016/j.petrol.2014.11.020, 2015.

1020 Thurston, G. D., and Spengler, J. D.: A quantitative assessment of source contributions to inhalable
1021 particulate matter pollution in metropolitan Boston, *Atmos. Environ.*, 19, 9-25, 10.1016/0004-
1022 6981(85)90132-5, 1985.

1023 Thurston, G. D., Ito, K., and Lall, R.: A source apportionment of U.S. fine particulate matter air pollution,
1024 Atmos. Environ., 45, 3924-3936, 10.1016/j.atmosenv.2011.04.070, 2011.

1025 Tokarek, T. W., Huo, J. A., Odame-Ankrah, C. A., Hammoud, D., Taha, Y. M., and Osthoff, H. D.: A gas
1026 chromatograph for quantification of peroxy-carboxylic nitric anhydrides calibrated by thermal
1027 dissociation cavity ring-down spectroscopy, Atmos. Meas. Tech., 7, 3263-3283, 10.5194/amt-7-3263-
1028 2014, 2014.

1029 Tokarek, T. W., Brownsey, D. K., Jordan, N., Garner, N. M., Ye, C. Z., Assad, F. V., Peace, A., Schiller, C. L.,
1030 Mason, R. H., Vingarzan, R., and Osthoff, H. D.: Biogenic Emissions and Nocturnal Ozone Depletion
1031 Events at the Amphitrite Point Observatory on Vancouver Island, Atmosphere-Ocean, 1-12,
1032 10.1080/07055900.2017.1306687, 2017.

1033 Wang, S. C., and Flagan, R. C.: Scanning electrical mobility spectrometer, Aerosol Sci. Technol., 13, 230-
1034 240, 10.1080/02786829008959441, 1990.

1035 Wang, X. L., Chow, J. C., Kohl, S. D., Percy, K. E., Legge, A. H., and Watson, J. G.: Characterization of
1036 PM_{2.5} and PM₁₀ fugitive dust source profiles in the Athabasca Oil Sands Region, J. Air Waste Manag.
1037 Assoc., 65, 1421-1433, 10.1080/10962247.2015.1100693, 2015.

1038 Wang, X. L., Chow, J. C., Kohl, S. D., Percy, K. E., Legge, A. H., and Watson, J. G.: Real-world emission
1039 factors for Caterpillar 797B heavy haulers during mining operations, Particuology, 28, 22-30,
1040 10.1016/j.partic.2015.07.001, 2016.

1041 Warren, L. A., Kendra, K. E., Brady, A. L., and Slater, G. F.: Sulfur Biogeochemistry of an Oil Sands
1042 Composite Tailings Deposit, Front. Microbiol., 6, 14, 10.3389/fmicb.2015.01533, 2016.

1043 Watson, J., Chow, J., Wang, X., Zielinska, B., Kohl, S., and Gronstal, S.: Characterization of real-world
1044 emissions from nonroad mining trucks in the Athabasca Oil Sands Region during September, 2009,
1045 2013.

1046 WBEA: WBEA annual report 2013, Wood Buffalo Environmental Association, 2013.

1047 Whaley, C., Makar, P. A., Shephard, M. W., Zhang, L., Zhang, J., Zheng, Q., Akingunola, A., Wentworth, G.
1048 R., Murphy, J. G., Kharol, S. K., and Cady-Pereira, K. E.: Contributions of natural and anthropogenic
1049 sources to ambient ammonia in the Athabasca Oil Sands and north-western Canada, Atmos. Chem.
1050 Phys., 18, 2011-2034, 10.5194/acp-18-2011-2018, 2017.

1051 Williams, B. J., Goldstein, A. H., Kreisberg, N. M., and Hering, S. V.: An in-situ instrument for speciated
1052 organic composition of atmospheric aerosols: Thermal Desorption Aerosol GC/MS-FID (TAG), Aerosol
1053 Sci. Technol., 40, 627-638, 10.1080/02786820600754631, 2006.

1054 Wilson, N. K., Barbour, R. K., Chuang, J. C., and Mukund, R.: Evaluation of a real-time monitor for fine
1055 particle-bound PAH in air, Polycycl. Aromat. Compd., 5, 167-174, 10.1080/10406639408015168,
1056 1994.

1057 Yeh, S., Jordaan, S. M., Brandt, A. R., Turetsky, M. R., Spatari, S., and Keith, D. W.: Land Use Greenhouse
1058 Gas Emissions from Conventional Oil Production and Oil Sands, Environm. Sci. Technol., 44, 8766-
1059 8772, 10.1021/es1013278, 2010.

1060 Zhang, Y., Wang, Y., Chen, G., Smeltzer, C., Crawford, J., Olson, J., Szykman, J., Weinheimer, A. J., Knapp,
1061 D. J., Montzka, D. D., Wisthaler, A., Mikoviny, T., Fried, A., and Diskin, G.: Large vertical gradient of
1062 reactive nitrogen oxides in the boundary layer: Modeling analysis of DISCOVER-AQ 2011
1063 observations, J. Geophys. Res.-Atmos., 121, 1922-1934, 10.1002/2015jd024203, 2016.

1064

1065